LAWRENCE
LIVERMORE
NATIONAL
LABORATORY

LLNL-JRNL-426782

Integrated Nucleosynthesis in Neutrino Driven Winds

L. F. Roberts, S. E. Woosley, R. D. Hoffman

April 1, 2010

The Astrophysical Journal

Disclaimer

UCRL-JRNL-426782

Integrated Nucleosynthesis in Neutrino Driven Winds

L. F. Roberts[1], S. E. Woosley[1], and R. D. Hoffman[2]

ABSTRACT

Although they are but a small fraction of the mass ejected in core-collapse supernovae, neutrino-driven winds (NDWs) from nascent proto-neutron stars (PNSs) have the potential to contribute significantly to supernova nucleosynthesis. In previous works, the NDW has been implicated as a possible source of r-process and light p-process isotopes. In this paper we present time-dependent hydrodynamic calculations of nucleosynthesis in the NDW which include accurate weak interaction physics coupled to a full nuclear reaction network. Using two published models of PNS neutrino luminosities, we predict the contribution of the NDW to the integrated nucleosynthetic yield of the entire supernova. For the neutrino luminosity histories considered, no true r-process occurs in the most basic scenario. The wind driven from an older $1.4M_{\odot}$ model for a PNS is moderately neutron-rich at late times however, and produces ^{87}Rb, ^{88}Sr, ^{89}Y, and ^{90}Zr in near solar proportions relative to oxygen. The wind from a more recently studied $1.27M_{\odot}$ PNS is proton-rich throughout its entire evolution and does not contribute significantly to the abundance of any element. It thus seems very unlikely that the simplest model of the NDW can produce the r-process. At most, it contributes to the production of the N = 50 closed shell elements and some light p-nuclei. In doing so, it may have left a distinctive signature on the abundances in metal poor stars, but the results are sensitive to both uncertain models for the explosion and the masses of the neutron stars involved.

Subject headings: nuclear reactions, nucleosynthesis, abundances, supernovae — stars: neutron

[1]Department of Astronomy and Astrophysics, University of California, Santa Cruz, CA 95064 USA

[2]Computational Nuclear Physics Group, L-414, Lawrence Livermore National Laboratory, Livermore, CA 94550 USA

1. Introduction

The site where r-process nuclei above A=90 have been synthesized remains a major unsolved problem in nucleosynthesis theory (e.g., Arnould et al. 2007). Historically, many possibilities have been proposed (see Meyer 1994), but today, there are two principal contenders - neutron star mergers (Lattimer et al. 1977; Freiburghaus et al. 1999) and the NDW (e.g. Woosley et al. 1994; Witti et al. 1994; Thompson et al. 2001; Wanajo et al. 2001; Arcones et al. 2007). Observations of ultra-metal-poor stars suggest that many r-process isotopes were already quite abundant at early times in the galaxy (Cowan et al. 1995; Sneden et al. 1996; Frebel et al. 2007), suggesting both a primary origin for the r-process and an association with massive stars. NDWs would have accompanied the first supernovae that made neutron stars and, depending upon what is assumed about their birth rate and orbital parameters, the first merging neutron stars could also have occurred quite early.

Both the merging neutron star model and the NDW have problems though. In the simplest version of galactic chemical evolution, merging neutron stars might be capable of providing the necessary integrated yield of the r-process in the sun, but they make it too rarely in large doses and possibly too late to be consistent with observations (Argast et al. 2004). On the other hand, making the r-process in NDWs requires higher entropies, shorter time-scales, or lower electron mole numbers, Y_e, than have been demonstrated in any realistic, modern model for a supernova explosion (though see Burrows et al. 2006).

Many previous papers and models of the neutrino driven wind have either focused on the production of nuclei heavier than iron using either greatly simplified dynamics (Beun et al. 2008; Farouqi et al. 2009) or focused on the dynamics while not including detailed nuclear physics (Qian & Woosley 1996; Otsuki et al. 2000; Arcones et al. 2007; Fischer et al. 2009; Huedepohl et al. 2009). Post processing nuclear network calculations have been performed using thermal histories from accurate models of the dynamics, but the calculations sampled only a limited set of trajectories in the ejecta (Witti et al. 1994; Woosley et al. 1994; Hoffman et al. 1997; Thompson et al. 2001) or did not include detailed weak interaction physics that sets the electron fraction in the ejecta (Wanajo et al. 2001; Wanajo 2006). No one has yet calculated the complete synthesis of a realistic NDW and combined it with the yields from the rest of the supernova.

To address this situation, and to develop a framework for testing the nucleosynthesis of future explosion models, we have calculated nucleosynthesis using neutrino luminosity histories taken from two PNS calculations found in the literature (Woosley et al. 1994; Huedepohl et al. 2009). This was done using a modified version of the implicit one-dimensional hydrodynamics code Kepler, which includes an adaptive nuclear network of arbitrary size. This network allows for the production of both r-process nuclei during neutron-rich phases of the wind and production of light p-elements during proton-rich phases. Since the results of wind nucleosynthesis depend sensitively on the neutrino luminosities and interaction rates (Qian & Woosley 1996; Horowitz 2002), we have included accurate neutrino interaction rates that contain both general relativistic and weak magnetism

corrections.

The synthesis of all nuclei from carbon through lead is integrated over the history of the NDW and combined with the yield from the rest of the supernova, and the result is compared with a solar distribution. If a nucleus produced in the NDW is greatly overproduced relative to the yields of abundant elements in the rest of the supernova, there is a problem. If it is greatly underproduced, its synthesis in the NDW is unimportant. If it is co-produced, the NDW may be responsible for the galactic inventory of this element. An important outcome of this study are the yields expected from a "plain vanilla" model for the NDW. Are there any elements that are robustly produced and thus might be used as diagnostics of the wind in an early generation of stars?

In §2, we discuss the general physics of neutrino driven winds and analytically delineate the regions in neutrino temperature space were different modes of nucleosynthesis occur. We then discuss our numerical model in §3. In §4, the results of the time dependent models are presented. We conclude with a discussion of how the NDW might affect galactic chemical evolution and consider if this allows the strontium abundance in low metallicity halo stars to be used as a tracer of supernova fallback at low metallicity. Finally, we discuss some possible modifications of the basic model that might improve the r-process production. These ideas will be explored more thoroughly in a subsequent paper.

2. General Concepts and Relevant Physics

After collapse and bounce in a core collapse supernova, a condition of near hydrostatic equilibrium exists in the vicinity of the neutrinospheres. The temperature of the outer layers is changing on a time scale determined by the Kelvin-Helmholtz time of the PNS, $\tau_{KH} \approx 10s$ (Burrows & Lattimer 1986; Pons et al. 1999). Heating and cooling in this atmosphere are dominated by the charged current processes $(\nu_e + n) \rightleftharpoons (e^- + p)$ and $(\bar{\nu}_e + p) \rightleftharpoons (e^+ + n)$ (Qian & Woosley 1996). Equating these rates, while neglecting the neutron-proton mass difference and weak magnetism corrections and assuming the geometry can be approximated as close to plane-parallel gives the temperature structure of the neutron star atmosphere as a function of radius, $T_{atm} \approx 1.01\,\mathrm{MeV}\, R_{\nu,6}^{-1/3} L_{\nu,51}^{1/6} \epsilon_{\nu,MeV}^{1/3} \left(y_\nu/y\right)^{1/3}$, where $L_{\nu,51}$ and $\epsilon_{\nu,MeV}$ are the electron neutrino luminosity and average neutrino energy at the neutrino sphere in units of 10^{51} ergs s^{-1} and MeV, respectively. The gravitational redshift factor is $y = \sqrt{1 - 2GM_{NS}/rc^2}$ which, when evaluated at the neutrino sphere, R_ν, is y_ν. Notice that the only dependence on radius is carried in the redshift factor, so that the atmosphere is close to isothermal.

At the radius, r_c, where the pressure in the envelope becomes radiation dominated, the material becomes unstable to outflow (Duncan et al. 1986). The density at which this wind begins can be found approximately by equating the radiation pressure to the baryonic pressure. This results in a critical density, $\rho_c \approx 8.3 \times 10^7\,\mathrm{g\,cm^{-3}}\, R_{\nu,6}^{-1} L_{\nu,51}^{1/2} \epsilon_{\nu,MeV} \left(y_\nu/y\right)$, at which significant outflow begins and the kinetic equilibrium of weak interactions ceases to hold. Under these conditions, nuclear

statistical equilibrium is maintained on a time scale much shorter than the dynamical time scale and, for these temperatures and densities, there will be no bound nuclei present. Since the electron fraction is set by kinetic equilibrium, the composition of the wind does not depend on any previous nuclear processing, so any nucleosynthesis from the wind will be primary.

Assuming that most neutrino heating occurs near r_c, the entropy is constant once the temperature cools to the nucleon recombination temperature, $kT \approx 0.5$ MeV. Therefore, the final nuclear abundances in the wind depend mainly on the wind entropy, electron fraction, and the dynamical timescale at the radius where alpha combination occurs (Qian & Woosley 1996). To determine the contribution of the wind to the nucleosynthesis of the entire supernova, the mass loss rate must also be known. Estimates for these quantities are given in the Appendix along with a discussion of the effect of general relativistic corrections.

Integrating the mass loss rate (equation A11) for a typical neutrino luminosity history implies that the wind will eject approximately $10^{-3}\,M_\odot$ of material. This in turn means that for the wind to contribute to the integrated yields of the supernova for a particular isotope, that isotope needs to overproduced relative to its solar mass fraction by a factor of at least 10^5 in the wind, assuming the rest of the supernova ejects $\sim 10\,M_\odot$ and has over production factors of its most abundant metals of order 10.

Using the analytic results for the wind dynamics and nucleosynthesis given in the Appendix (equations A6, A8, A11, A16,B1, B4, B10, and using the neutrino interaction rates given in §3.1 to fix the thermodynamic state at r_c), one can easily explore the neutrino temperature parameter space to determine the neutrino temperatures and fluxes that are most conducive to the r-process or the production of the light p-process. Figure 1 is a neutrino two-color plot where it is assumed that the deleptonization rate is zero and that the neutrino luminosity scales with the temperature to the fourth power ($L_{\nu_e,tot} = 10^{51}(\langle T_\nu \rangle / 3.5\,\mathrm{MeV})^4\,\mathrm{ergs}^{-1}$). The different nucleosynthetic regions are delineated by the final calculated neutron to seed ratio. To give a feeling for how a particular point in parameter space might contribute to the integrated nucleosynthesis of the wind, the mass loss rate is also shown. The analytic models results are compared with those of our detailed numerical calculations in figures 4 & 11.

For a significant amount of material to move past the N = 50 closed shell during neutron-rich conditions, the anti-neutrino temperature must be approximately 60% higher than the neutrino temperature. For second peak r-process nucleosynthesis to occur, the asymmetry must be greater than 100%. Modern PNS cooling calculations do not give such large asymmetries (Pons et al. 1999; Huedepohl et al. 2009).

Under proton-rich conditions, only a small region of the parameter space at high neutrino and low anti-neutrino temperature is favorable for the νp-process. There will be a small amount of neutron production in the white region, but it is unlikely that significant production of the light p-process elements ^{74}Se, ^{78}Kr, ^{84}Sr, and ^{92}Mo will occur. The region in neutrino temperature space where there is significant neutron production is unlikely to be reached. This region is small due to

the short dynamical time scale of the wind, which reduces the time over which anti-neutrinos can capture on free neutrons. One should note that, very soon after shock formation in the supernova, a wind solution may not be appropriate and material will be entrained closer to the PNS for a longer period of time. This scenario would be similar to the the conditions used in Pruet et al. (2006).

Therefore, based upon simple principles, it seems unlikely that the standard wind scenario will produce r-process or light p-process isotopes in solar ratios, as is required by observations of metal poor halo stars (Sneden et al. 1996). This same conclusion has been reached by other authors (Witti et al. 1994; Hoffman et al. 1997; Thompson et al. 2001), but is repeated here in simple terms. We will find that our numerical calculations give similar results and that there is no significant r-process nucleosynthesis associated with the wind. Still, the wind can produce some isotopes that may have an observable signature. For standard PNS luminosities, the wind will spend a significant amount of time in the region of parameter space were N = 50 closed shell nucleosynthesis occurs.

3. Computational Method

To more accurately investigate the integrated nucleosynthesis of the NDW, we have updated the implicit Lagrangian hydrodynamics code Kepler (Weaver et al. 1978; Woosley et al. 2002) to carry out time-dependent simulations of the wind dynamics and nucleosynthesis. Kepler has been used previously to study time-independent winds(Qian & Woosley 1996), but the weak and nuclear physics employed there was rudimentary and nucleosynthesis was not tracked. Trajectories from Kepler were used for post-processing calculations of nucleosynthesis in Hoffman et al. (1997).

Kepler solves the non-relativistic hydrodynamic equations in Lagrangian coordinates assuming spherical symmetry. First order general relativistic corrections are included in the gravitational force law (cf. Shapiro & Teukolsky (1983)). All order v/c effects are neglected. This is justified since the maximum wind speeds encountered are, at most, a few percent of the speed of light. The momentum equation is then

$$\frac{dv_r}{dt} = -4\pi r^2 \frac{\partial P}{\partial m} - \frac{Gm}{r^2}\left(1 + \frac{P}{\rho c^2} + \frac{4\pi P r^3}{mc^2}\right)\left(1 - \frac{2Gm}{rc^2}\right)^{-1} \quad (1)$$

where the symbols have their standard meanings. As has been shown by previous studies (Qian & Woosley 1996; Cardall & Fuller 1997; Otsuki et al. 2000; Thompson et al. 2001), general relativistic corrections to the gravitational force can have an appreciable effect on the entropy and dynamical time scale of the wind. The equation of state includes a Boltzmann gas of nucleons and nuclei, an arbitrarily relativistic and degenerate ideal electron gas, and photons.

3.1. Weak Interaction Physics

Energy deposition from electron neutrino capture on nucleons, neutrino annihilation of all neutrino flavors, and neutrino scattering of all flavors on electrons is included in the total neutrino heating rate. Neutrino "transport" is calculated in the light-bulb approximation. The energy deposition rate is dominated by neutrino captures on nucleons. The neutrino annihilation rates given in Janka (1991) are employed. For the scattering rates, the rates given in Qian & Woosley (1996) are used, but we include general relativistic corrections. Standard neutrino capture rates are employed in the limit of infinitely heavy nucleons with first order corrections. In this limit, the cross section is (Y.Z. Qian, private communication)

$$\sigma_{\substack{\nu n \\ \bar{\nu} p}} = \frac{G_F^2 cos^2(\theta_C)}{\pi(\hbar c)^4} \left[g_V^2 + 3g_A^2\right] (\epsilon_\nu \pm \Delta)^2 \left(1 \pm W_{M,\substack{\nu \\ \bar{\nu}}} \epsilon_\nu\right) \tag{2}$$

Here, G_F is the Fermi coupling constant, θ_C is the Cabibo angle, g_V and g_A are the dimensionless vector and axial-vector coupling constants for nucleons, Δ is the proton neutron mass difference, ϵ_ν is the neutrino energy, and $W_{M,\substack{\nu \\ \bar{\nu}}}$ accounts for the weak magnetism and recoil corrections to the neutrino-nucleon cross section when the base cross section is derived in the limit of infinitely heavy nucleons (Horowitz 2002). This correction reduces the anti-neutrino cross section and increases the neutrino cross section (by about a total of 10% at the energies encountered in NDWs), which, for a given incident neutrino spectrum, significantly increases the asymptotic electron fraction. Assuming a thermal distribution, these cross sections result in the neutrino energy deposition rate for anti-electron neutrino capture

$$\begin{aligned} \dot{q}_{\bar{\nu}p} = & \quad 4.2 \times 10^{18} \text{ergs s}^{-1}\text{g}^{-1} \tfrac{Y_p L_{\bar{\nu},51}}{\langle\mu\rangle r_6^2} \\ \times & \quad \Big[-W_M^{\bar{\nu}p} \tfrac{\langle\epsilon_{\bar{\nu}}^4\rangle}{\langle\epsilon_{\bar{\nu}}\rangle} + (1 + 2W_M^{\bar{\nu}p}\Delta) \tfrac{\langle\epsilon_{\bar{\nu}}^3\rangle}{\langle\epsilon_{\bar{\nu}}\rangle} \\ & -(2\Delta + W_M^{\bar{\nu}p}\Delta^2) \tfrac{\langle\epsilon_{\bar{\nu}}^2\rangle}{\langle\epsilon_{\bar{\nu}}\rangle} + \Delta^2\Big] \end{aligned} \tag{3}$$

and a similar expression for electron neutrino capture. The neutrino energy distributions are parameterized by assuming a Fermi-Dirac spectrum. The neutrino energy averages, $\langle\epsilon_\nu^n\rangle$, are evaluated using this distribution. The neutrino energy moments and luminosity are evaluated in the rest frame of the fluid. With general relativistic corrections for the bending of null geodesics, the average neutrino angle is given by

$$\langle\mu\rangle = \frac{1}{2} + \frac{1}{2}\sqrt{1 - \left(\frac{R_\nu y_\nu}{ry}\right)^2}. \tag{4}$$

Special relativistic corrections are negligible in the regions where neutrino interactions are important.

The lepton capture rates used are calculated in the limit of infinitely heavy nucleons. This results in a positron capture energy loss rate

$$\begin{aligned} \dot{q}_{e^+n} = & \quad 6.9 \times 10^{15} \text{ ergs g}^{-1}\text{ s}^{-1}\, Y_n T_{10}^6 \\ \times & \quad \int_0^\infty du f_e(u, -\eta) \left(u^5 + 3\delta u^4 + 3\delta^2 u^3 + \delta^3 u^2\right) \end{aligned} \tag{5}$$

here $f_e(u,\eta) = (\exp(u-\eta)+1)^{-1}$, η is the electron degeneracy parameter, δ is the proton neutron mass difference divided by k_bT, and Y_n is the neutron fraction. A similar rate is employed for electron capture.

For the neutrino losses, we include electron and positron capture on nucleons and include thermal losses as tabulated in Itoh et al. (1996). The energy loss rate in the wind is dominated by the electron captures.

3.2. Nuclear Physics

During a hydrodynamic time step in Kepler, the nuclear energy generation rate and the changing nuclear composition are calculated using a modified version of the 19-isotope network described in Weaver et al. (1978). Neutrino and electron capture rates on nucleons are coupled to the network, which are calculated under the same assumptions as the charged current energy deposition/loss rates described above. Therefore, non-equilibrium evolution of the electron fraction is accurately tracked.

Although this network is appropriate for calculating energy generation throughout the entire wind, it is not large enough to accurately track the nucleosynthesis once alpha recombination begins at $T \approx 0.5$ MeV. Therefore, for temperatures below 20GK an adaptive network is run alongside the hydrodynamics calculation. The details of this network can be found in Woosley et al. (2004) and Rauscher et al. (2002). As a fluid element passes the temperature threshold, the composition from the 19-isotope network is mapped into the adaptive network. Typically, the network contains approximately 2000 isotopes. Where available, experimental nuclear reaction rates are employed, but the vast majority of the rates employed in the network come from the statistical model calculations of Rauscher & Thielemann (2000). In general, the nuclear physics employed in these calculations is the same as that used in Rauscher et al. (2002). The nucleon weak interaction rates employed in the 19-isotope network are also used in the adaptive network.

3.3. Problem Setup and Boundary Conditions

To start the neutrino driven wind problem, an atmosphere of mass 0.01 $M_\odot$ is allowed to relax to hydrostatic equilibrium on top of a fixed inner boundary at the neutron stars radius. The mass enclosed by the inner boundary is the neutron star's mass. The photon luminosity from the neutron star is assumed to be nearly Eddington, but we have found that the properties of the wind are insensitive to the the luminosity boundary condition. Once hydrostatic equilibrium is achieved, the neutrino flux is turned on and a thermal wind forms. This wind is allowed to relax to a quasi-steady state, and then the 19 isotope network is turned on and the wind is, once again, allowed to reach a quasi-steady state. After this point, the neutrino flux is allowed to vary with time, and the adaptive network is turned on.

As the calculation proceeds, the mass of the envelope being followed decreases and could eventually all be blown away. To prevent this, mass is added back to the innermost mass elements at a rate equal to the mass loss rate in the wind. The mass added to a fluid element at each time step is a small fraction of its total mass. We find that mass recycling has no effect on the properties of the wind. It is simply a way of treating a problem that is essentially Eulerian in a Lagrangian code.

For most runs, a zero outer boundary pressure and temperature are assumed. To investigate the effect of a wind termination shock, a time dependent outer boundary condition is included in some of the simulations detailed below. The pressure of the radiation dominated region behind the supernova shock is approximately given by (Woosley et al. 2002)

$$P_{ps} \approx \frac{E_{sn}}{4\pi(v_{sn}t)^3} \tag{6}$$

where E_{sn} is the explosion energy of the supernova, v_{sn} is the supernova shock velocity, and t is the time elapsed since the shock was launched. As was discussed in Arcones et al. (2007), this results in a wind termination shock at a radius where the condition $\rho_w v_w^2 + P_w \approx P_{ps}$ obtains, where v_w is the wind velocity and ρ_w is the wind density. To avoid an accumulation of too many zones, mass elements are removed from the calculation once they exceed a radius of $10,000\,\mathrm{km}$. This is well outside the sonic point and nuclear burning has ceased by this radius in all calculations .

4. Numerical Results

To survey both low and intermediate mass core collapse supernovae, neutrino emission histories were taken from two core collapse calculations, one from a $20M_\odot$ (Woosley et al. 1994) supernova calculation and the other from a $8.8M_\odot$ (Huedepohl et al. 2009) supernova calculation. Since the PNSs studied have significantly different masses and neutrino emission characteristics, one is able to get a rough picture of how integrated nucleosynthesis in the NDW varies with progenitor mass.

4.1. Neutrino Driven Wind from a $20M_\odot$ Supernova

The first set of neutrino luminosities and temperatures are taken from Woosley et al. (1994). This calculation began with a $20M_\odot$ progenitor meant to model the progenitor of 1987A (Woosley et al. 1988). The resulting neutron star had a gravitational mass of $1.4M_\odot$ and the neutrino sphere was taken to be at 10 km. The neutrino luminosities and average energies as a function of time from this model are shown in figure 2. After about 4 seconds, the neutrino energies become constant and the large difference between the electron neutrino and anti-neutrino energies implies that the wind will be neutron rich. This supernova model had some numerical deficiencies (Sam Dalhed, Private Communication). We also note that, unlike more modern 1-D supernova models of $\sim 20M_\odot$ stars (e.g. Fischer et al. 2009), this model resulted in a successful explosion when a mixing length theory

prescription for convection was included. The entropy calculated for the wind in Woosley et al. (1994) ($S/N_A k \approx 400$) were unrealistically large due to some problems with the equation of state. Here, that is not so important because the NDW is being calculated separately, but this study did rely on older neutrino interaction rates and did not include weak magnetism corrections (see §3.1). Therefore, the results obtained using these neutrino histories are only suggestive of what might happen in a more massive star. If weak magnetism were taken into account, the calculated electron and anti-electron neutrino temperatures would probably be somewhat further apart.

The calculation was run for a total of 18 seconds. During this time, the mass loss rate decreased by almost three orders of magnitude while a total mass of $2 \times 10^{-3} M_\odot$ was lost in the wind. A snapshot of the wind structure two seconds after bounce is shown in figure 3. Note that the wind velocity stays very sub-luminal throughout the calculation. Therefore, the neglect of special relativistic effects is reasonable. The secondary bump in the energy deposition rate occurs at the same radius where nucleons and alpha-particles assemble into heavy nuclei. This increases the entropy by about 10 units. Clearly, the electron fraction is set interior to were nuclei form. The radius where nuclei form is at a large enough value that the alpha effect (Fuller & Meyer 1995) is not significant at early times in the wind. However, as the neutrino luminosity decreases with time, nucleon recombination occurs at a smaller radius, and the alpha effect becomes increasingly important.

The time evolution of the wind as calculated by Kepler is shown in figure 4. The increase in asymptotic entropy is mainly driven by the decrease in neutrino luminosity, since the average neutrino energies do not vary greatly. The analytic approximation (calculated using equation A8 and the neutrino interaction rates given in §3.1) to the entropy tracks the entropy calculated in Kepler fairly well. This implies that the variation in the neutrino luminosity with time does not significantly alter the dynamics from a steady state wind. In contrast to the high entropies reported in Woosley et al. (1994), the entropy here never exceeds 130. For the time scales and electron fractions also obtained, such a low value of entropy is not sufficient to give a strong r-process (see below).

The electron neutrino and anti-neutrino energies do move further apart as a function of time though, which causes the wind to evolve from proton-rich conditions at early times to neutron-rich conditions later. A transition occurs from the synthesis of proton-rich isotopes via the νp-process at early times to the $\alpha-$process mediated by the reaction sequence $\alpha(\alpha\mathrm{n},\gamma)^9\mathrm{Be}(\alpha,\mathrm{n})^{12}\mathrm{C}$ later. The slight difference between the analytic approximation and the Kepler calculation of Y_e is due to the alpha effect (Fuller & Meyer 1995).

Integrated production factors for the wind are shown in figure 5. The production factor for the species i is defined as

$$P_i = \frac{X_{i,w} M_w}{X_{i,\odot}(M_w + M_{sn})}, \tag{7}$$

where $X_{i,w}$ is the mass fraction of species i in the wind after all material has decayed to stable isotopes, M_w is the mass ejected in the wind, and M_{sn} is the amount of mass ejected by the entire

supernova. $X_{i,\odot}$ is the mass fraction of isotope i in the sun for which the values of Lodders (2003) were used. The only isotopes that are co-produced in the wind alone are ^{87}Rb, ^{88}Sr, ^{89}Y, and ^{90}Zr, with production factor of ^{88}Sr about a factor of 3 higher than the other two N = 50 closed shell isotopes. If neutrons are exhausted at high temperatures when charged particle reactions are occurring, the wind will mainly produce the isotopes ^{88}Sr, ^{89}Y, and ^{90}Zr (Hoffman et al. 1997). This happens when the condition

$$\frac{\bar{Z}}{\bar{A}} \approx 0.42 - 0.49 = \frac{Y_e f_\alpha}{2Y_e(f_\alpha - 1) + 1} \tag{8}$$

is met. Here, $f_\alpha \approx 14Y_s/Y_{\alpha,i}$ is the fraction of the initial helium abundance that gets processed into heavy nuclei.

Before eight seconds, the production factors had been much closer. After eight seconds though, the wind is dominated by ^{88}Sr because $Y_e \sim 0.45$ and only 53% of alpha particles are free after freeze out which puts $\frac{\bar{Z}}{\bar{A}} \approx 0.41$ for heavy nuclei just below the range given in equation 8. There are not enough free neutrons to make any significant amount of heavier nuclei, and this results in significant production of the stable N = 50 closed shell isotope with the lowest $\frac{\bar{Z}}{\bar{A}}$.

During the first four seconds, the wind is proton rich and the isotopes ^{69}Ga, ^{70,72}Ge, ^{74,76}Se, and ^{78,80,82}Kr are produced by proton captures on seed nuclei produced by the triple-alpha reaction and subsequent (α,p) reactions. Although the mass loss rate is much higher when the wind is proton rich, the alpha-fraction freezes out at 98% of its initial value, which results in significantly decreased production of heavy nuclei. The difference in final alpha fraction between the neutron- and proton-rich phases of the wind is due mainly to the difference in speed of the reaction chains $\alpha(2\alpha,\gamma)^{12}$C and $\alpha(\alpha\text{n},\gamma)^9\text{Be}(\alpha,\text{n})^{12}$C, but also to the decreased entropy at early times.

We can compare this with the analytic predictions for nucleosynthesis by plotting the neutrino temperature evolution from this model on a neutrino "two-color plot" (figure 6). Here we have set $L_{\bar{\nu}_e} = 1.2L_\nu$ which is approximately correct at late times in the calculation of Woosley et al. (1994). The wind never reaches a region in which r-process nucleosynthesis is expected, but spends a significant amount of time making nuclei in the N = 50 closed shell isotones.

4.1.1. Variations in Neutrino Properties

Since the neutrino temperatures from the original model were uncertain, several other models were calculated. One had a reduced (by 15%) electron antineutrino temperature; another had the weak magnetism corrections to the neutrino interaction rates turned off. A smaller antineutrino temperature is more in line with recent calculations of PNS cooling (Pons et al. 1999; Keil et al. 2003). Because the model of Woosley et al. (1994) did not include weak magnetism corrections, our model with weak magnetism corrections turned off is more consistent with the original supernova model.

The production factors for the model with a reduced electron antineutrino temperature are shown in figure 7. The yield of ^{88}Sr is reduced by almost a factor of ten from the base case, while the production factors of ^{89}Y and ^{90}Zr are reduced by a factor of three. In this case, the wind also produces the proton-rich isotopes ^{74}Se, ^{78}Kr, and ^{84}Sr. The coproduction line for lighter elements like oxygen in a $20M_{\odot}$ supernova at solar metallicity is around 18, so the wind could contribute to the total nucleosynthesis if the antineutrino temperature was reduced, but its contribution would be small.

The yields when weak magnetism corrections are ignored are shown in figure 8. Without weak magnetism, the electron fraction drops below 0.4 at late times when the entropy is fairly high. Equation 8 is no longer satisfied and material moves past the N = 50 closed shell towards A $\approx$ 110. Some r-process isotopes are produced, such as ^{96}Zr and ^{100}Mo, but not anywhere near solar ratios, and no material reaches the first r-process peak.

4.1.2. Effect of a Wind Termination Shock

To investigate the possible effect of a wind termination shock on nucleosynthesis, another model was run with a boundary pressure and temperature determined by equation 6. An explosion energy of 10^{51} erg was assumed and the shock velocity was taken as 2×10^9 cm s^{-1}. This resulted in a wind termination shock that was always at a radius greater than 10^3 km. Similar to the simulation without a wind termination shock, the N=50 closed shell elements dominate the wind's nucleosynthesis.

The main difference between the case with and without a wind termination shock is a shift in the mass of isotopes produced during the proton-rich phase. During this phase, the post shock temperature varied from 2.5 GK down to 0.8 GK and the density varied from 5×10^4 g cm^{-3} to 5×10^2 g cm^{-3}. These conditions are very favorable for continued proton capture once the long lived waiting point isotopes ^{56}Ni and ^{64}Ge are bypassed by (n,p) reactions. Because these conditions persist for at least a second after a fluid element passes through the wind termination shock, significantly more proton captures can occur on seed nuclei that have moved past mass ~ 64 relative to the case with no termination shock. Still, not many more neutrons are produced per seed nucleus relative to the base run. Therefore, the net number of seeds that get past the long lived waiting points remains small and the proton-rich wind does not contribute to the integrated nucleosynthesis. It should also be noted that a different treatment of the wind's interaction with the supernova shock might result in a breeze solution which may supply more favorable conditions for νp-process nucleosynthesis (Wanajo 2006).

4.1.3. Total Supernova Yields

In figure 9, the production factors from a $20M_{\odot}$ supernova model from Woosley & Weaver (1995) have been combined with the production factors we calculated in the NDW with the unaltered neutrino histories of (Woosley et al. 1994) with weak magnetism corrections included. The wind could be responsible for synthesizing the isotopes ^{87}Rb, ^{88}Sr, ^{89}Y, and ^{90}Zr. ^{88}Sr production is above the co-production band, but the rest are in agreement with the stellar yields. This overproduction of ^{88}Sr is similar to the result of Hoffman et al. (1997).

For the model with a reduced anti-electron neutrino temperature combined with the yields from the $20M_{\odot}$ supernova model, the wind contributes 28%, 42%, 35%, 75%, 75%, and 80% of the total ^{74}Se, ^{78}Kr, ^{84}Sr, ^{88}Sr, ^{89}Y, and ^{90}Zr abundances in the supernova model, respectively. This wind model does not result in any isotopes being overproduced relative to the rest of the yields of the supernova. For the case with weak magnetism turned off, the nuclei produced by the wind are overproduced relative to those made in the rest of the star by factor of nearly 100, hence this would need to be a very rare event if this model were realistic.

Since the progenitor model used in Woosley et al. (1994) was a model for SN 1987A, we have also combined the abundances calculated in the wind those predicted by Woosley et al. (1988). ^{88}Sr, produced by the NDW, dominates the elemental strontium yield. For the base NDW model, [Sr/Fe]= 0.8, if weak magnetism corrections are neglected, [Sr/Fe]= 1.6; and if the anti-neutrino temperature is reduced in the base model by 15%, [Sr/Fe]= 0.2.

Clearly, weak magnetism corrections and variations in the neutrino temperatures have a very significant effect on nucleosynthesis in the wind. Aside from the effects of an extra source of energy (5.2), the neutrino spectra are the largest current theoretical uncertainty in models of the NDW.

4.2. Neutrino Driven Wind from a $8.8M_{\odot}$ Supernova

The second PNS model is a more modern one-dimensional calculation of an electron-capture supernova (Huedepohl et al. 2009) that started from an $8.8M_{\odot}$ progenitor model (Nomoto 1984). This resulted in a PNS with a gravitational mass of $1.27M_{\odot}$ and a radius of 15 km. Together the lower mass and increased radius imply a lower gravitational potential at the neutrinosphere. This work employed neutrino interaction rates which took weak magnetism and "in-medium" effects into account. The neutrino luminosities and average energies as a function of time are shown in figure 10. The maximum difference between the electron and anti-electron neutrino average energies is significantly less than in the model of Woosley et al. (1994). This is likely due in part to both the decreased gravitational potential of the PNS and the more accurate neutrino interaction rates in the newer model.

The calculation was run for a total of nine seconds, at which point the mass loss rate had dropped by two orders of magnitude. The total amount of mass ejected in the wind was $3.8 \times$

$10^{-4}\,M_\odot$. In figure 11, the properties of the NDW calculated using Kepler are plotted as a function of time. Notice that the entropy never reaches above 100 in this model, which diminishes the likelihood of significant nucleosynthesis. For comparison, we also include the analytic estimates detailed above. There is reasonable agreement between the analytic and the numerical calculations, but not nearly as good as in the $20M_\odot$ model.

In contrast to the simulation run with the neutrino luminosities of Woosley et al. (1994), the electron fraction continues to increase with time. The difference between the average electron neutrino energy and electron anti-neutrino energy is, at most, about 3 MeV, compared to a maximum of 8 MeV in the Woosley et al. (1994) calculations. Also, the difference between the average neutrino energies decreases as a function of time, compared to an increase with time in Woosley et al. (1994). Finally, the energies of all kinds of neutrinos are lower in the Huedepohl et al. (2009) calculation, so that the proton-neutron rest mass difference significantly suppresses the anti-neutrino capture rate relative to the neutrino capture rate. These differences are presumably due to both the different neutron star masses and neutrino interaction rates employed.

The conditions in this model thus preclude *any* r-process nucleosynthesis, but they are potentially favorable for production of some low mass p-process isotopes by the νp-process. The integrated isotopic production factors are shown in figure 12. The total ejected mass was take as 7.4 $M_\odot$, as 1.4 $M_\odot$ neutron star is left behind in the calculation of Huedepohl et al. (2009). During the calculation a maximum network size of 988 isotopes is reached. The p-process elements ^{74}Se and ^{78}Kr are co-produced with ^{63}Cu, ^{67}Zn, and ^{69}Ga, but the maximum production factor for any isotope is 1 when weighted with the total mass ejected in the supernova. Therefore, in this simple model, the proton-rich wind from low mass neutron stars will not contribute significantly to galactic chemical evolution.

The entropies encountered when the mass loss rate is high are low (~ 50), so that there is more production of ^{56}Ni by triple-alpha and a subsequent αp-process. As the neutron abundance available for the νp-process is given by

$$Y_n \approx \frac{\lambda_\nu Y_p}{\rho N_A \sum_i Y_i \langle \sigma v \rangle_{i(n,p)j}}, \tag{9}$$

increased seed production reduces the available neutron abundance and therefore hinders production of the p-process elements ^{74}Se, ^{78}Kr, ^{84}Sr, and ^{92}Mo. Additionally, at early times, the dynamical time scale is short which implies a smaller integrated neutron to seed ratio, Δ_n (see the appendix).

The yields of from this model cannot be combined with the yields from the rest of the supernova because they are not published. As Nomoto (1984) has discussed, the mass inside the helium burning shell was close to the mass of the neutron star that was left after the explosion. Therefore the ejecta of the supernova is expected to have small production factors. This implies that, even when the yields of the NDW are combined with the rest of the supernova, it is unlikely that these low mass core collapse supernovae will contribute significantly to galactic chemical evolution.

4.2.1. Effect of a Wind Termination Shock

As was mentioned above, it is very possible that a transonic wind solution may not be appropriate this early in the supernovas evolution. Fischer et al. (2009) have found that a wind termination shock is not present in a one-dimensional supernova model using the progenitor from Nomoto (1984). Still, it is interesting to consider the effect of a reverse shock on the wind nucleosynthesis.

A second simulation was run with a time dependent boundary pressure given by equation 6, with $E_{sn} = 10^{50}$ erg and $v_{sn} = 2 \times 10^9$ cm s^{-1}. This results in a wind termination shock at a radius of approximately 3×10^8 cm throughout the simulation. Inside the wind termination shock the wind dynamics are very similar to those in the run with no boundary pressure. There is almost no difference in the nucleosynthesis in the runs with and without a wind termination shock.

After 0.75 s, the post shock temperature drops below 1 GK and the wind termination shock has little effect on subsequent nucleosynthesis. Because the post shock temperature is high for less than one second, the wind termination shock has very little effect on the integrated nucleosynthesis. A larger explosion energy would likely result in a larger effect on the nucleosynthesis, but there are still very few neutrons available to bypass the long lived waiting points and it seems unlikely that the production factors would be increased by more than a factor of a few.

5. Discussion

5.1. Strontium and Yttrium in Halo Stars

Since strontium and yttrium are abundantly produced in our models, it may be that the NDW has contributed to their production throughout cosmic history. An interesting possibility is that the abundances of these elements might trace the birth rate of neutron stars at an early time. Taking a standard r-process abundance pattern from metal poor stars with strong r-process enhancments, Travaglio et al. (2004) find that 8% and 18% of solar strontium and yttrium, respectively, are not produced by either the "standard" r-process or any component of the s-process. It therefore seems plausible that charged particle reactions in the NDW could make up this "missing" component.

Any nucleosynthesis that happens in the NDW will be primary, i.e. provided that the mass function of neutron stars at birth does not itself scale with metallicity, similar nucleosynthesis will occur for stars of any population. Below [Fe/H]~ -1.5, no component of the s-process contributes to the abundances of N = 50 closed shell isotopes (Serminato et al. 2009). If the NDW escapes the potential well of the PNS, and contributes to the galactic budget of N = 50 closed shell isotopes, it should provide a floor to [Sr/Fe] and [Y/Fe]. Based upon the arguments of Travaglio et al. (2004), this floor would be at [Sr/Fe]≈ -0.18 and [Y/Fe]≈ -0.16. These numbers assume that when the main r-process source contributes in addition to the NDW, [Sr/Fe] and [Y/Fe] approach their solar values even though the s-process has yet to contribute. This is consistent with observations.

In defining this floor, one must assume that the abundances in a particular star sample a large number of individual supernovae. This is because the production of N=50 closed shell elements likely depends on the PNS mass and therefore the progenitor mass. As we have found, [Sr/Fe]= 0.8 in the $20M_{\odot}$ model with reduced anti-neutrino temperatures, but the $8.8M_{\odot}$ model produces no strontium. Observations show that below [Fe/H]~ -3, the spreads in [Sr/Fe] and [Y/Fe] increase significantly and the mean values falloff some (François et al. 2007; Cohen et al. 2008; Lai et al. 2008). Single stars have values of [Sr/Fe] below the predicted floor. This could be because, at this metallicity, the metals in a particular star come from only a handful of supernovae.

Another possible explanation of this variation is that supernova fall back varies with metallicity. Since the NDW is the innermost portion of the supernova ejecta, it will be the most susceptible to fallback. It has been found that the amount of supernova fallback depends strongly on the metallicity of the progenitor, especially going between zero and low metallicity (Zhang et al. 2008). Additionally, mixing is also greatly reduced in zero metallicity stars compared to solar metallicity stars due to the formers compact structure (Joggerst et al. 2009).

The current understanding of supernova fallback suggests that the nucleosynthetic contribution of the NDW will be suppressed at very low metallicity. Of course, the ejection of iron by the supernova is also very susceptible to fallback, so the effect of fallback on the evolution of [Sr,Y/Fe] is complicated and may require fine tuning to give the observed decrease. A somewhat different explanation was offered by Qian & Wasserburg (2008) who attributed the fall off of [Sr/Fe] at low metallicity to the evolution of the "hypernova" rate with metallicity. For their purposes, hypernovae were stellar explosions that contributed iron without making much strontium.

Given the sensitivity of strontium and yttrium yields to uncertain NDW characteristics, especially neutrino fluxes and temperatures, it may be some time before the complex history of these elements is even qualitatively understood. It is likely though that their abundances in halo stars will ultimately be powerful constraints upon the evolution of supernova physics as a function of metallicity.

5.2. Possible Modifications of the Basic Model

As is clear from figures 5 and 12, the simplest case of a non-magnetic non-rotating NDW from a neutron star without additional energy deposition does not produce r-process nuclei in significant abundances. Are there extensions to this simple scenario that *could* make the wind a site of the r-process?

As was pointed out by Metzger et al. (2007), the combination of rotation and magnetic fields can decrease the dynamical time scale by magnetic "flinging". This is not particularly effective. Adding a non-thermal source of kinetic energy means that less thermal energy must be put into the wind for it to escape the potential well. Therefore, lower entropies are achieved. It seems unlikely that this mechanism, by itself, will salvage the NDW as a site for the full r-process. If there were a

way to make the rotation rate of the PNS high enough, it might be possible that there would be a centrifugally driven outflow. Then the electron fraction would be determined by kinetic equilibrium much deeper in the PNS envelope, and the material in the outflow would have an electron fraction much lower than that seen in the wind.

To test this possibility, we ran calculations with a centrifugal force term added and corotation with the PNS enforced out to 10^3 km. Unfortunately, for reasonable PNS spin rates (20 ms period), we found this had little effect on the nucleosynthesis. These calculations were in a regime were the electron fraction was still set by neutrino interactions.

Many authors have discussed the possible effects of both matter-enhanced(Qian & Fuller 1995; Sigl 1995) and collective neutrino (Pastor & Raffelt 2002; Duan et al. 2006) oscillations on NDW nucleosynthesis. If electron antineutrinos could undergo a collective oscillation near the launch radius while the electron neutrinos did not, this would increase the average energy of the antineutrinos if the μ and τ neutrinos have a significantly higher temperature, facilitating a reduction in the electron fraction. For a normal mass hierarchy however, matter enhanced neutrino oscillations would probably cause electron neutrino flavor conversion, which would *increase* the electron fraction and decrease the probability of significant r-process nucleosynthesis (Qian & Fuller 1995).

Collective neutrino oscillations can cause antineutrino oscillations in the region were the electron fraction is set, and thereby decrease the electron fraction where pure MSW oscillations would have predicted an increased electron fraction(Duan et al. 2006). Clearly, the main effect of oscillations would be on the composition of the wind, not the dynamics. As can be seen in the neutrino two color plots, oscillations would have to change the effective temperature of the anti-neutrinos by a very large amount to move from a region where N=50 close shell nucleosynthesis occurs to a region where the second r-process peak can be produced.

These effects are based upon the assumption that μ- and τ-neutrinos are significantly more energetic than the electron neutrinos. In the calculation of Woosley et al. (1994), this is the case, as can be seen in figure 2. Interestingly, the μ and τ temperatures are almost the same as the electron anti-neutrino temperature in the Huedepohl et al. (2009) calculation, which can be seen in figure 10. It is not clear wether this difference obtains because of the difference in the PNS masses or the significantly different neutrino physics employed in the calculations. A detailed study of neutrino transport in static backgrounds showed that the inclusion of all relevant neutrino interactions brings the average energies of the μ- and τ- neutrinos closer to the temperature of the anti-electron neutrinos (Keil et al. 2003). Therefore it is uncertain wether or not neutrino oscillations could effect nucleosynthesis significantly. Clearly, the uncertainties here are not in the wind itself but in the formation of the spectra in the PNS and the details of neutrino transport with neutrino oscillations.

Finally, it has been suggested (Takahashi et al. 1994; Qian & Woosley 1996; Suzuki & Nagataki 2005) that adding a secondary source of volumetric energy deposition can significantly increase the entropy of the wind, which results in a more alpha-rich freeze out and conditions that would be

more favorable for r-process nucleosynthesis. The addition of energy to the wind also decreases the dynamical timescale. Since the important quantity to consider for the r-process is s^3/τ_d (Hoffman et al. 1997), both effects increase the chance of having a significant neutron to seed ratio after freeze out. If the NDW model is to be salvaged, this seems to us the minimal necessary extension. Of course, the physical process contributing this extra energy is very uncertain. One possibility is that oscillations of the PNS power sound waves which produce shocks and deposit energy in the wind, similar to the supernova mechanism of Burrows et al. (2006), but smaller in magnitude. We will explore this possibility in some detail in a subsequent paper.

6. Conclusions

We have performed calculations of the dynamics and nucleosynthesis in time dependent neutrino driven winds. This was done for two sets of neutrino spectra calculated in one-dimensional supernova models taken from the literature. The nucleosynthesis in these models was compared with supernova yields to determine if these models were consistent with observations. Additionally, we compared the results of these numerical models to analytic models of the neutrino driven wind and found good agreement.

Similar to most of the work on the NDW after Woosley et al. (1994), we find that it is unlikely that the r-process occurs in the neutrino driven wind unless there is something that causes significant deviation from a purely neutrino driven wind. Additionally, in the simplest case, there is little production of p-process elements at early times in the wind. In our calculation that used spectra from a more massive neutron star, the wind only produces the N=50 closed shell elements ^{87}Rb, ^{88}Sr, ^{89}Y, and ^{90}Zr.

This result is sensitive to small changes in the neutrino interaction rates (i.e. the inclusion of weak magnetism) and changes to the neutrino temperature of order 10%. We also find that the effect of a wind termination shock on the wind nucleosynthesis is small.

Using neutrino spectra from an $8.8 M_\odot$ supernova that drives a wind which is proton rich throughout its duration (Huedepohl et al. 2009), we find that no significant νp-process occurs and the wind does not contribute to the yields of the supernova. The neutrino spectra from this model are probably more accurate than the spectra from the model of Woosley et al. (1994). We also investigated the effect of an outer boundary pressure which resulted in a wind termination shock. This had a negligible effect on the nucleosynthesis.

However, one also expects that the nucleosynthesis in the NDW will vary considerably from event to event, especially with the mass and possibly the rotation rate of the PNS. The winds from more massive PNS have greater entropy and might, in general, be expected to produce heavier elements and more of them. The neutrino spectral histories of PNS as a function of mass have yet to be determined over a wide range of parameter space. Currently, the neutrino luminosities and temperatures are the largest uncertainties in models of the NDW.

We would like to thank Alex Heger, David Lai, Enrico Ramirez-Ruiz, Sanjay Reddy, and Yong-Zhong Qian for useful discussions about issues relating to this work. L. R. was supported by an NNSA/DOE Stewardship Science Graduate Fellowship (DE-FC52-08NA28752) and the University of California Office of the President (09-IR-07-117968-WOOS). S. W. was supported by the US NSF (AST-0909129), the University of California Office of the President (09-IR-07-117968-WOOS), and the DOE SciDAC Program (DEFC-02-06ER41438). R. H. was supported by the DOE SciDAC Program (DEFC-02-06ER41438) and under the auspices of the Department of Energy at Lawrence Livermore National Laboratory under contract DE-AC52-07NA27344.

A. Analytic Wind Dynamics

To understand the wind dynamics, we follow arguments similar to those of Qian & Woosley (1996) and Cardall & Fuller (1997). Conservation of the stress-energy tensor and number flux in a Schwarzschild geometry in steady state leads to the wind equations in critical form

$$\dot{M} = 4\pi r^2 m_b n \gamma y v \tag{A1}$$

$$\gamma y v \frac{d}{dr} \ln(\gamma y h_r) = \frac{\dot{q} m_b}{c^2 h_r} \tag{A2}$$

$$\gamma^2 \left(v^2 - c_s^2\right) \frac{dv}{dr} = \frac{v}{r}\left[2c_s^2 - \frac{GM}{ry^2}\left(1 - \frac{c_s^2}{c^2}\right)\right] - \frac{\dot{q} m_b}{3\gamma y h_r} \tag{A3}$$

here $\dot{M}$ is the rest mass loss rate, m_b is the baryon mass, n is the baryon number density, v is the velocity measured by an observer at rest in the Schwarzschild frame, $\gamma = \left(1 - v^2/c^2\right)^{-1/2}$, $\dot{q}$ is the neutrino heating rate per mass, c_s is the sound speed, M is the neutron star mass, $h_r = 1 + \epsilon/(m_b c^2) + P/(n m_b c^2)$, P is the pressure, and ϵ is the energy per baryon not including the rest mass. To fully describe the wind, these equations must be supplemented by a set of nuclear rate equations and an equation of state. For our analytic calculations we used a radiation-dominated non-degenerate equation of state comprised of relativistic electrons, positrons, and photons.

First, we estimate where the critical radius (i.e. the radius where radiation pressure equals the nucleon gas pressure) sits in relation to the neutrino sphere. Neglecting the temperature gradient in the equation of hydrostatic balance gives the density structure of the atmosphere,

$$\log(n(r)/n_c) \approx -\int_{r_l}^{r} dr \frac{GM m_b}{r^2 y^2 T(r)} \tag{A4}$$

The optical depth of this atmosphere for neutrinos is

$$\tau = \sigma_\nu(\epsilon_\nu) \int_r^\infty \frac{n}{y} \approx \sigma_\nu(\epsilon_\nu) n_c \int_r^\infty \frac{dr}{y} \exp\left(-\int_{r_l}^{r} dr' \frac{GM m_b}{r'^2 y'^2 T(r')}\right) \tag{A5}$$

Taking the neutrinosphere to be at an optical depth of 2/3, the gas pressure equal to the radiation pressure at the critical radius, and approximating gravity as constant throughout the envelope, we

arrive at an equation for the critical radius

$$r_c \approx R_\nu \left[1 + \frac{T_c}{g m_b R_\nu} \ln\left(\frac{2}{3\tau_0} y_\nu\right)\right] \tag{A6}$$

where $\tau_0 = \sigma_\nu(\epsilon_\nu) n_c T_c / g m_b$. For characteristic values of L_ν, ϵ_ν, R_ν, and M, r_c is only a few percent larger than R_ν. This implies that the GR corrections to the neutrino interaction rates at r_c will be at most a few percent. For characteristic values, the GR correction to gravity will be $y(r_l)^{-2} \approx y_\nu^{-2} \approx 1.5$. This agrees with the observation made by previous authors that GR corrections to gravity dominate over corrections to the neutrino interaction rates (Cardall & Fuller 1997; Thompson et al. 2001).

Assuming that most neutrino heating occurs near r_c, the entropy can be considered constant once the temperature cools to the nucleon recombination temperature ($T \approx 0.5$ MeV). Therefore, the final nuclear abundances in the wind depend mainly on the wind entropy, electron fraction, and the timescale for outflow (Qian & Woosley 1996; Hoffman et al. 1997). To determine the contribution of the wind to the nucleosynthesis of the entire supernova, the mass loss rate must also be known. We now find estimates for these quantities and for the transonic radius of the wind.

To determine the asymptotic entropy, the total energy deposition per baryon needs to be estimated. Using equation A2 and assuming the asymptotic velocity is small, the total energy deposited per baryon is

$$\ln(\gamma_f) - \ln(y_c h_c) \approx -\ln(y_c h_c) \approx \int_{r_\nu}^{\infty} dr \frac{\dot{q} m_b}{\gamma y v c^2 h_r} \approx \int_{r_c}^{\infty} dr \frac{\dot{q}_\nu m_b}{\gamma y v c^2 h_r} = Q/(m_b c^2) \tag{A7}$$

Considering that most of the neutrino energy is deposited near the hydrostatic atmosphere, the final entropy per baryon is approximately

$$s_f = \int_{r_\nu}^{\infty} dr \frac{\dot{q} m_b}{\gamma y v T} \approx \int_{r_c}^{\infty} dr \frac{\dot{q}_\nu m_b}{\gamma y v T} + s_c \approx -\frac{m_b c^2 \ln(h_c y_c) h_{r,c}}{T_c} + s_c \tag{A8}$$

Assuming that the neutron-proton rest mass difference is negligible, the entropy of the envelope is negligible, and taking the relativistic enthalpy outside the logarithm to be one results in the scaling relation

$$s_f \approx 464 \ln\left(y_c^{-2}\right) R_{\nu,6}^{1/3} L_{\nu,51}^{-1/6} \epsilon_{\nu,MeV}^{-1/3} \left(\frac{y_c}{y_\nu}\right)^{1/3}. \tag{A9}$$

Notice that all the general relativistic corrections, both due to gravity and to the neutrino interaction rates, increase the entropy from the non-relativistic case (Cardall & Fuller 1997; Otsuki et al. 2000). As was discussed above, the dominant correction to the newtonian case is from the GR correction to gravity.

To fix the mass loss rate, we must estimate the velocity at the critical radius. Taking the momentum equation in critical form and assuming approximate hydrostatic equilibrium and subsonic

velocities gives $c_s^2 dv/dr \approx \frac{\dot{q}}{3\gamma y}$. Assuming that acceleration has occurred over a scale height, we have

$$y v_c \approx \frac{h_{eff}\dot{q}(r_c)}{6c_s^2} \tag{A10}$$

where the heating rate at the critical radius is divided by two to account for the fact that beneath the critical radius the net heating goes to zero over approximately a scale height so that a characteristic value of the heating rate is one half the heating rate at the critical radius. The scale height is given by $h_{eff}^{-1} = (\rho + P)GM/Pr^2y^2$. Combining these with equation A1 results in a mass loss rate of

$$\dot{M} \approx 4\pi r_c^4 \frac{P}{\rho + P} y_c^2 \frac{m_b n_c \dot{q}_\nu(r_c)}{3GMc_{s,c}^2} \tag{A11}$$

Using our result for the entropy gives a scaling relation for the mass loss rate,

$$\dot{M} \approx 7.4 \times 10^{-11}\,\mathrm{M}_\odot\,\mathrm{s}^{-1}\,\frac{r_{l,6}^4 L_{\nu,51}^{5/3}\epsilon_{\nu,MeV}^{10/3}}{R_{\nu,6}^{10/3}\,(M/M_\odot)\ln\left(y_l^{-2}\right)} y_l^2 \left(\frac{y_\nu}{y_l}\right)^{10/3}. \tag{A12}$$

Notice that GR corrections reduce the mass loss rate significantly, by about a factor of 2. Only including GR effects on neutrino propagation and energies decreases the mass loss rate by about 10%. The reduced mass loss rate due to GR corrections does effect the integrated nucleosynthetic yields, although the effect is not as great as the effect of the GR corrections on the entropy.

Given the entropy and the mass loss rate, we can solve for the evolution of temperature with radius outside of the heating region where the velocity is still small using the relation $\ln(h_r y) = \ln(y_c h_{r,c}) + Q \approx 0$, which gives

$$r \approx \frac{2GM}{c^2}\left[1 - (1 + Ts_f/m_b)^{-2}\right]^{-1} \tag{A13}$$

The dynamical timescale of the wind is defined by $\tau_d^{-1} = v\gamma y/n\,|dn/dr|$. Steady state baryon number conservation yields

$$\frac{1}{n}\left|\frac{dn}{dr}\right| = \frac{2}{r} + \frac{\gamma^2}{v}\frac{dv}{dr} + \frac{GM}{r^2y^2} \tag{A14}$$

Neutrino energy deposition will no longer dominate the momentum equation when nucleons reform, but the velocity will be subsonic. In this limit, the momentum equation yields

$$\frac{\gamma^2}{v}\frac{dv}{dr} = \frac{GM}{r^2y^2c_s^2}\left(1 - c_s^2\right) - \frac{2}{r} \tag{A15}$$

which results in an estimate for the dynamical timescale far inside the sonic point,

$$\tau_d^{-1} \approx \frac{G\dot{M}M}{4\pi r^4 n m_b y^2 c_s^2} \tag{A16}$$

For seed formation we are interested in the dynamical timescale around 2 MeV. Combining with our result for the temperature structure of the atmosphere we have

$$\tau_{d,2} \approx \frac{16\pi(GMm_b)^3 m_b K}{9 s_f^4 \dot{M}} y^2 \tag{A17}$$

$$\approx 8.2\,\mathrm{ms} \left(\frac{M}{1.4 M_\odot}\right)^3 \left(\frac{s_f}{100}\right)^{-4} \left(\frac{\dot{M}}{10^{-5} M_\odot\,\mathrm{s}^{-1}}\right)^{-1} y^2 \tag{A18}$$

To agree with the definition of the dynamical timescale given in Qian & Woosley (1996), this should be multiplied by three as our definition of τ_d differs slightly from the one used in Qian & Woosley (1996). We note that all of the scaling relations above are equivalent to those of Qian & Woosley (1996) in the non-relativistic limit.

From this discussion, it is unclear if a transsonic wind will obtain. A reasonable criteria for transsonic solutions is that $\rho v^2 + P$ at the sonic point is greater than the pressure behind the supernova shock, which is approximately given by equation 6. Equation A3 along with equation of state for the wind can be combined to give the temperature and sound speed at the sonic radius in terms of the sonic radius and known quantities

$$T_s = \frac{3GM_{NS}m_b}{2r_s s_f y_s^2 \left(1 + \frac{GM_{NS}}{2r_s y_s^2 c^2}\right)} \tag{A19}$$

This results in an implicit equation for the sonic radius

$$\dot{M} \approx r_s^{-3/2} \frac{16\pi m_b^{1/2} K}{3^{3/2} s_f^{1/2}} y_s \gamma_s \left(\frac{3GM_{NS}m_b}{2 s_f y_s^2 \left(1 + \frac{GM_{NS}}{2r_s y_s^2 c^2}\right)}\right)^{7/2} \tag{A20}$$

where K is the radiation constant for photons and leptons combined. In the non-relativistic limit, the sonic radius reduces to

$$r_s \approx 860\,\mathrm{km} \left(\frac{s_f}{100}\right)^{-8/3} \left(\frac{M_{NS}}{1.4 M_\odot}\right)^{7/3} \left(\frac{\dot{M}}{10^{-5} M_\odot\,\mathrm{s}^{-1}}\right)^{-2/3}. \tag{A21}$$

The wind termination shock position is approximately given by (Arcones et al. 2007)

$$R_{rs} \approx 1.3 \times 10^3\,\mathrm{km} \left(\frac{\dot{M}}{10^{-5} M_\odot\,\mathrm{s}^{-1}}\right)^{1/2} \left(\frac{R_s}{10^9\,\mathrm{cm}}\right)^{3/2} \left(\frac{E_{sn}}{10^{51}\,\mathrm{erg}}\right)^{-1/2} \left(\frac{v_w}{10^9\,\mathrm{cm\ s}^{-1}}\right)^{1/2} \tag{A22}$$

where E_{sn} is the supernova explosion energy, R_s is the radius of the supernova shock, and v_w is the wind velocity just inside the wind termination shock.

B. Analytic Wind Nucleosynthesis

The electron fraction in the wind is given by kinetic equilibrium of neutrino interaction rates at the critical radius, as the temperature has decreased enough that lepton capture is unimportant (Qian & Woosley 1996)

$$Y_{e,f} \approx \frac{\lambda_{\nu_e}}{\lambda_{\nu_e} + \lambda_{\bar{\nu}_e}} \tag{B1}$$

where λ_{ν_e} is the neutrino capture rate per baryon and $\lambda_{\bar{\nu}_e}$ is the anti-neutrino capture rate per baryon. After weak interactions cease and the temperature has decreased about 0.5 MeV, alpha particles form in the wind. The initial alpha number fraction is $Y_{\alpha,i} \approx Y_e/2$ for neutron-rich conditions and $Y_{\alpha,i} \approx 1/2 - Y_e/2$ for proton-rich conditions.

In both proton and neutron-rich winds, the nucleosynthesis will be characterized by the neutron to seed ratio in the wind. For winds with $Y_e >\approx 0.5$, alpha particles recombine into ^{12}C by the standard triple alpha reaction and then experience alpha particle captures up to approximately mass 56 (Woosley & Hoffman 1992). The slowest reaction in this sequence is ^{4}He(2α,γ)^{12}C, so the total number of seed nuclei produced is equal to the number of ^{12}C nuclei produced. The rate of alpha destruction is given by

$$\frac{dY_\alpha}{d\tau} \approx -14\rho_0^2 Y_\alpha^3 \lambda_{3\alpha} \tag{B2}$$

where $\rho_0 = m_b n$ is the rest mass density and $\lambda_{3\alpha}$ is the rate of triple alpha, which includes double counting factors. The factor of 14 comes from assuming alpha captures stop at ^{56}Ni. In general, we define an abundance by $n_i = nY_i$, where n_i is the number density of species i and n is the baryon density. Using our definition of the dynamical timescale, we have $d\tau \approx -\frac{\tau_d}{3T} dT$. Transforming Y_α to a function of temperature makes the integral given above trivial to solve. Using a rate for triple-alpha from Caughlan & Fowler (1988) and assuming the reaction flow stops at ^{56}Ni results in a seed abundance at the end of the α-process given by

$$Y_s \approx \frac{1 - Y_e}{28}\left(1 - \left[1 + 1.4 \times 10^5 \tau_d s_f^{-2}(1 - Y_e)^2\right]^{-1/2}\right) \tag{B3}$$

where s_f^{-2} enters because $\rho_0 \propto T^3/s_f$ for a radiation dominated equation of state and the density enters to the second power.

Under proton-rich conditions, the νp-process has the potential to occur. This process is similar to the rp-process, except that long lived beta-decays are bypassed by (n,p) reactions. An estimate for the integrated number of free neutrons produced is $\tau_d \lambda_{\bar{\nu}_e}(T_9 \approx 2)$, so that the neutron to seed ratio is

$$\Delta_n \approx \tau_d \lambda_{\bar{\nu}_e}(T_9 \approx 2)\frac{Y_p}{Y_s}. \tag{B4}$$

Here, $\lambda_{\bar{\nu}_e}(T_9 \approx 2)$ is the neutrino capture rate at the seed formation radius. A similar relation is found in Pruet et al. (2006). Although it is hard to estimate its effect, we note that the presence of a reverse shock can significantly affect the νp-process nucleosynthesis, as passage through the reverse shock slows the outward flow and rarefaction of the wind. Additionally, it increases the

temperature to close to the post supernova shock temperature. At early times for characteristic explosion energies, the wind is shock heated to a temperature of a few GK. This all combines to give a longer period of time over which proton capture on heavy nuclei is efficient and allows the νp-process to continue to higher mass than it would if no wind termination shock were present.

In the neutron-rich case, seed nuclei are produced by the slightly different reaction sequence ^{4}He(αn,γ)^{9}Be(α,n)^{12}C (Woosley & Hoffman 1992). For the conditions encountered in the wind, neutron catalyzed triple-alpha proceeds about ten times as quickly as ^{4}He(2α,γ)^{12}C. This implies that there will be a larger seed number than in proton-rich conditions. The rate of helium destruction is given by the equations (Hoffman et al. 1997)

$$\frac{dY_\alpha}{d\tau} \approx -\frac{\bar{Z}}{2}\rho_0 Y_\alpha Y_9 \lambda_{\alpha,n}(^9\mathrm{Be}) \tag{B5}$$

$$\frac{dY_n}{dY_\alpha} \approx \frac{2(\bar{A}-2\bar{Z})}{\bar{Z}} \tag{B6}$$

$$Y_9 = \frac{27}{32}N_a^2\left(\frac{2\pi\hbar^2}{m_b}\right)^3 Y_n Y_\alpha^2 \rho_0^2 T^{-3}\exp((B_9-2B_\alpha)/T) \tag{B7}$$

where $\bar{Z}$ is the average proton number of the seed nuclei, $\bar{A}$ is the average nucleon number of the seed nuclei, N_a is Avogadro's number, Y_α is the alpha particle abundance, Y_n is the neutron abundance, Y_9 is the ^{9}Be abundance, $\lambda_{\alpha,n}(^9\mathrm{Be})$ is the rate of ^{9}Be destruction by (α, n), and B_α and B_9 are the binding energies of ^{4}He and ^{9}Be, respectively. For $\lambda_{\alpha,n}(^9\mathrm{Be})$, we employ the rate given in Wrean et al. (1994). This set of equations can be solved analytically by once again transforming from proper time to temperature using the dynamical timescale. The resulting implicit expression for the final alpha fraction is somewhat cumbersome, so we do not reproduce it here. The seed abundance in terms of the initial and final alpha fraction is

$$Y_s = 2\frac{Y_{\alpha,i}-Y_{\alpha,f}}{\bar{Z}} \tag{B8}$$

the final neutron fraction is given by

$$Y_{n,f} = (1-2Y_e) - 2\frac{\bar{A}-2\bar{Z}}{\bar{Z}}\left(Y_{\alpha,i}-Y_{\alpha,f}\right) \tag{B9}$$

so that the neutron to seed ratio is

$$\Delta_n = \frac{\bar{Z}(1/2-Y_e)}{Y_e/2-Y_{\alpha,f}} + 2\bar{Z} - \bar{A}. \tag{B10}$$

The seed abundance at the end of charged particle reactions can be estimated by (Hoffman et al. 1997)

$$Y_s \approx \frac{1-2Y_e}{10}\left(1-\exp\left[-8\times10^8\tau_d s_f^{-3}Y_e^3\right]\right) \tag{B11}$$

where it has been assumed that the neutron abundance is what limits the reaction. Notice that the seed abundance in the proton-rich case depends on the entropy squared because it is mediated by an effective three body reaction, but in the neutron-rich case the entropy enters to the third power because of the effective four body interaction that mediates seed production.

REFERENCES

Arcones, A., Janka, H., & Scheck, L. 2007, A&A, 467, 1227

Argast, D., Samland, M., Thielemann, F., & Qian, Y. 2004, A&A, 416, 997

Arnould, M., Goriely, S., & Takahashi, K. 2007, Phys. Rep., 450, 97

Beun, J., McLaughlin, G. C., Surman, R., & Hix, W. R. 2008, Phys. Rev. C, 77, 035804

Burrows, A., & Lattimer, J. M. 1986, ApJ, 307, 178

Burrows, A., Livne, E., Dessart, L., Ott, C. D., & Murphy, J. 2006, ApJ, 640, 878

Cardall, C. Y., & Fuller, G. M. 1997, ApJ, 486, L111+

Caughlan, G. R., & Fowler, W. A. 1988, Atomic Data and Nuclear Data Tables, 40, 283

Cohen, J. G., Christlieb, N., McWilliam, A., Shectman, S., Thompson, I., Melendez, J., Wisotzki, L., & Reimers, D. 2008, ApJ, 672, 320

Cowan, J. J., Burris, D. L., Sneden, C., McWilliam, A., & Preston, G. W. 1995, ApJ, 439, L51

Duan, H., Fuller, G. M., Carlson, J., & Qian, Y. 2006, Phys. Rev. D, 74, 105014

Duncan, R. C., Shapiro, S. L., & Wasserman, I. 1986, ApJ, 309, 141

Farouqi, K., Kratz, K., Mashonkina, L. I., Pfeiffer, B., Cowan, J. J., Thielemann, F., & Truran, J. W. 2009, ApJ, 694, L49

Fischer, T., Whitehouse, S. C., Mezzacappa, A., Thielemann, F., & Liebendörfer, M. 2009, ArXiv e-prints

François, P., et al. 2007, A&A, 476, 935

Frebel, A., Christlieb, N., Norris, J. E., Thom, C., Beers, T. C., & Rhee, J. 2007, ApJ, 660, L117

Freiburghaus, C., Rosswog, S., & Thielemann, F. 1999, ApJ, 525, L121

Fuller, G. M., & Meyer, B. S. 1995, ApJ, 453, 792

Hoffman, R. D., Woosley, S. E., & Qian, Y.-Z. 1997, ApJ, 482, 951

Horowitz, C. J. 2002, Phys. Rev. D, 65, 043001

Huedepohl, L., Mueller, B., Janka, H., Marek, A., & Raffelt, G. G. 2009, ArXiv e-prints

Itoh, N., Hayashi, H., Nishikawa, A., & Kohyama, Y. 1996, ApJS, 102, 411

Janka, H. 1991, A&A, 244, 378

Joggerst, C. C., Woosley, S. E., & Heger, A. 2009, ApJ, 693, 1780

Keil, M. T., Raffelt, G. G., & Janka, H. 2003, ApJ, 590, 971

Lai, D. K., Bolte, M., Johnson, J. A., Lucatello, S., Heger, A., & Woosley, S. E. 2008, ApJ, 681, 1524

Lattimer, J. M., Mackie, F., Ravenhall, D. G., & Schramm, D. N. 1977, ApJ, 213, 225

Lodders, K. 2003, ApJ, 591, 1220

Metzger, B. D., Thompson, T. A., & Quataert, E. 2007, ApJ, 659, 561

Meyer, B. S. 1994, ARA&A, 32, 153

Nomoto, K. 1984, ApJ, 277, 791

Otsuki, K., Tagoshi, H., Kajino, T., & Wanajo, S. 2000, ApJ, 533, 424

Pastor, S., & Raffelt, G. 2002, Physical Review Letters, 89, 191101

Pons, J. A., Reddy, S., Prakash, M., Lattimer, J. M., & Miralles, J. A. 1999, ApJ, 513, 780

Pruet, J., Hoffman, R. D., Woosley, S. E., Janka, H., & Buras, R. 2006, ApJ, 644, 1028

Qian, Y., & Fuller, G. M. 1995, Phys. Rev. D, 52, 656

Qian, Y., & Wasserburg, G. J. 2008, ApJ, 687, 272

Qian, Y.-Z., & Woosley, S. E. 1996, ApJ, 471, 331

Rauscher, T., Heger, A., Hoffman, R. D., & Woosley, S. E. 2002, ApJ, 576, 323

Rauscher, T., & Thielemann, F. 2000, Atomic Data and Nuclear Data Tables, 75, 1

Serminato, A., Gallino, R., Travaglio, C., Bisterzo, S., & Straniero, O. 2009, Publications of the Astronomical Society of Australia, 26, 153

Shapiro, S. L., & Teukolsky, S. A. 1983, Black holes, white dwarfs, and neutron stars: The physics of compact objects

Sigl, G. 1995, Phys. Rev. D, 51, 4035

Sneden, C., McWilliam, A., Preston, G. W., Cowan, J. J., Burris, D. L., & Armosky, B. J. 1996, ApJ, 467, 819

Suzuki, T. K., & Nagataki, S. 2005, ApJ, 628, 914

Takahashi, K., Witti, J., & Janka, H. 1994, A&A, 286, 857

Thompson, T. A., Burrows, A., & Meyer, B. S. 2001, ApJ, 562, 887

Travaglio, C., Gallino, R., Arnone, E., Cowan, J., Jordan, F., & Sneden, C. 2004, ApJ, 601, 864

Wanajo, S. 2006, ApJ, 647, 1323

Wanajo, S., Kajino, T., Mathews, G. J., & Otsuki, K. 2001, ApJ, 554, 578

Weaver, T. A., Zimmerman, G. B., & Woosley, S. E. 1978, ApJ, 225, 1021

Witti, J., Janka, H., & Takahashi, K. 1994, A&A, 286, 841

Woosley, S. E., et al. 2004, ApJS, 151, 75

Woosley, S. E., Heger, A., & Weaver, T. A. 2002, Reviews of Modern Physics, 74, 1015

Woosley, S. E., & Hoffman, R. D. 1992, ApJ, 395, 202

Woosley, S. E., Pinto, P. A., & Weaver, T. A. 1988, Proceedings of the Astronomical Society of Australia, 7, 355

Woosley, S. E., & Weaver, T. A. 1995, ApJS, 101, 181

Woosley, S. E., Wilson, J. R., Mathews, G. J., Hoffman, R. D., & Meyer, B. S. 1994, ApJ, 433, 229

Wrean, P. R., Brune, C. R., & Kavanagh, R. W. 1994, Phys. Rev. C, 49, 1205

Zhang, W., Woosley, S. E., & Heger, A. 2008, ApJ, 679, 639

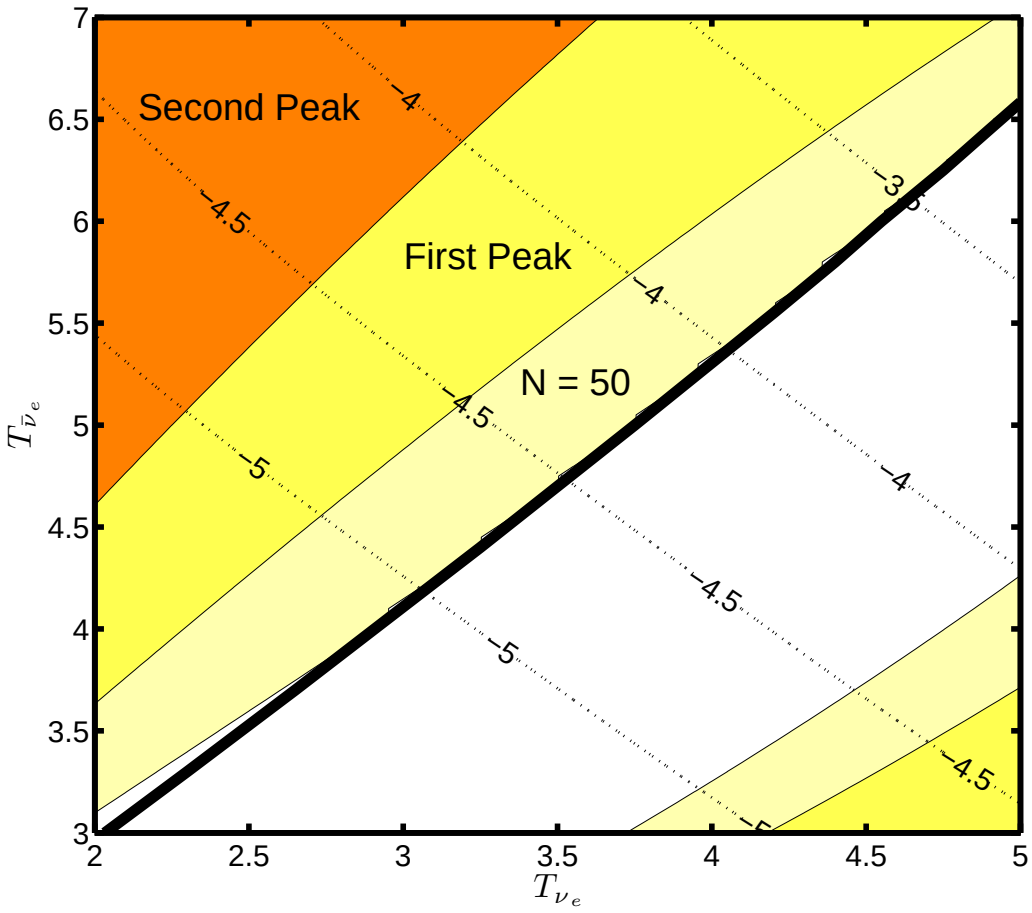

Fig. 1.— Neutrino two-color plot produced using the analytic relations in the Appendix. A neutron star with gravitational mass 1.4 $M_\odot$ has been assumed with a neutrinosphere radius of 10 km. The total neutrino luminosity is assumed to scale as $L_{\nu_e,tot} = 10^{51}(\langle T_\nu \rangle / 3.5\,\mathrm{MeV})^4\,\mathrm{ergs}^{-1}$. This luminosity is split between neutrinos and anti-neutrinos so as to ensure that the net deleptonization rate of the PNS is zero. The thick black line corresponds to an electron fraction of $Y_e = 0.5$. Above this line, neutron-rich conditions obtain and below it the matter is proton-rich. The white region is where there no free neutrons remain after charged particle reactions cease. The N = 50 (tan) region corresponds to final neutron-to-seed ratios between 0.01 and 15. The "first peak" (yellow) region corresponds to a neutron-to-seed ratio between 15 and 70, and the "second peak" (orange) region is where the neutron-to-seed ratio is greater than 70. The dashed lines correspond to the base ten logarithm of the mass loss rate in solar masses per second.

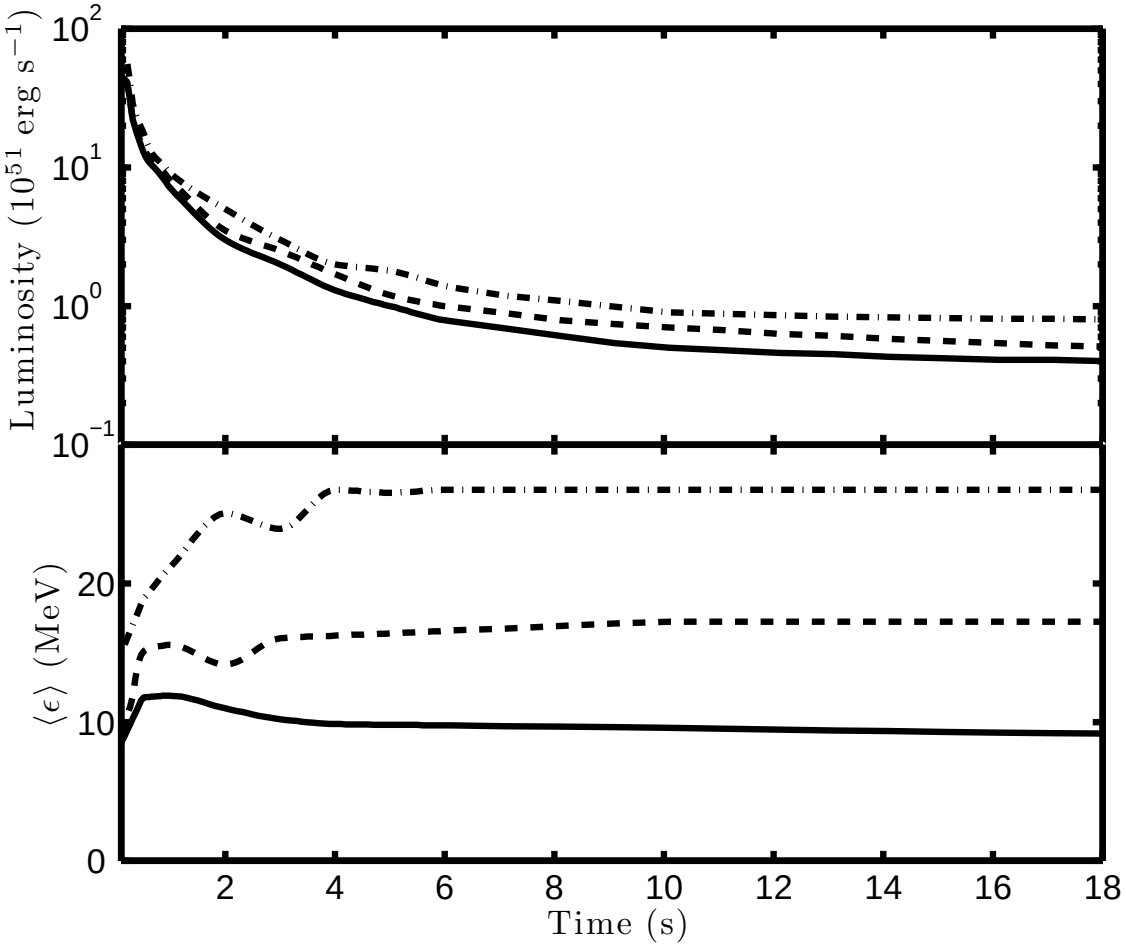

Fig. 2.— Neutrino luminosities and temperatures taken from the model of Woosley et al. (1994). The top panel is the neutrino luminosities. The bottom panel is the average neutrino energies. The solid line corresponds to ν_e, the dashed line corresponds to $\bar{\nu}_e$, the dot-dashed line corresponds to $\nu_{\mu,\tau}$.

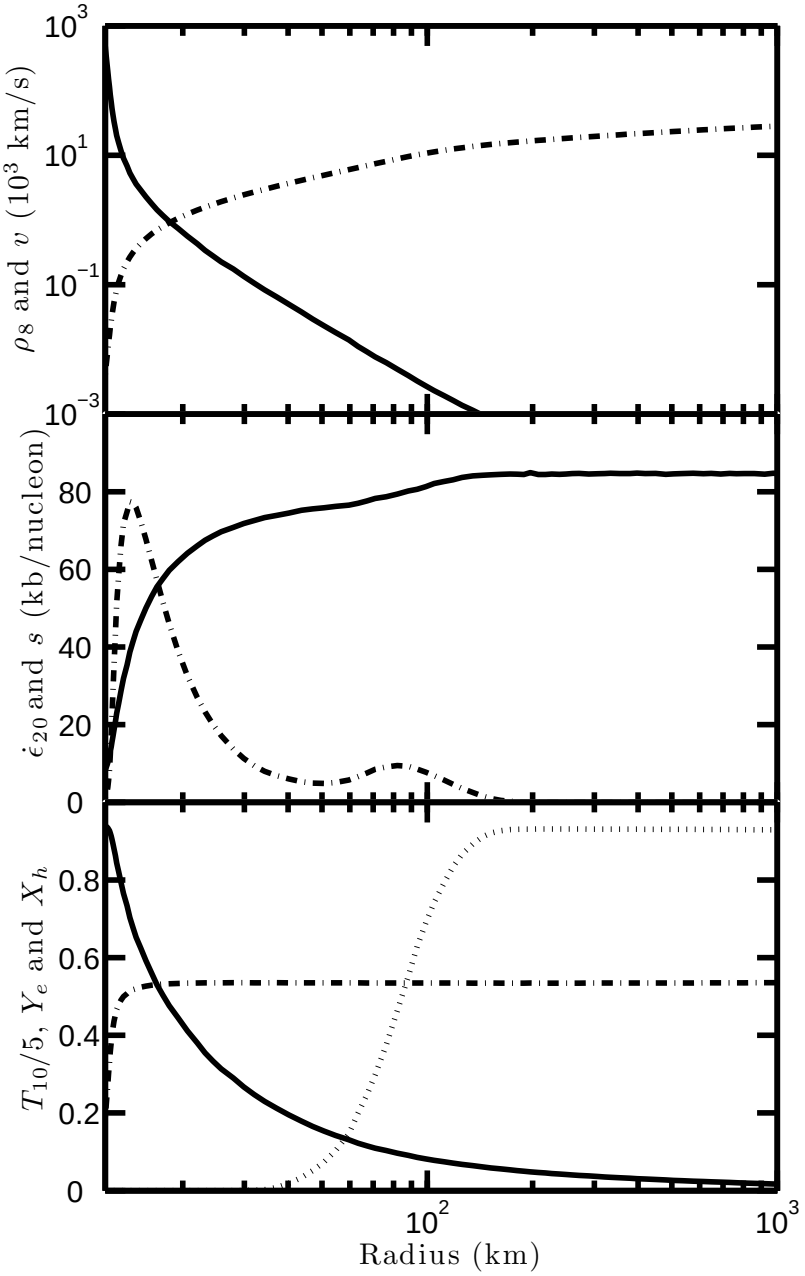

Fig. 3.— Wind structure after two seconds in the model using the neutrino luminosities from Woosley et al. (1994). The top panel shows the density in units of $10^8\,\mathrm{g\,cm^{-3}}$ (solid line) and the radial velocity in units of $10^3\,\mathrm{km\,s^{-1}}$ (dot-dashed line). The middle panel shows the net energy deposition rate from weak and strong interactions in units of $10^{20}\,\mathrm{erg\,g^{-1}\,s^{-1}}$ (dot-dashed line) and the entropy (solid line). The bottom panel shows the temperature in units of $5\times10^{10}\,\mathrm{K}$ (solid line), the electron fraction (dot-dahsed line), and the fraction of material contained in nuclei (dotted line).

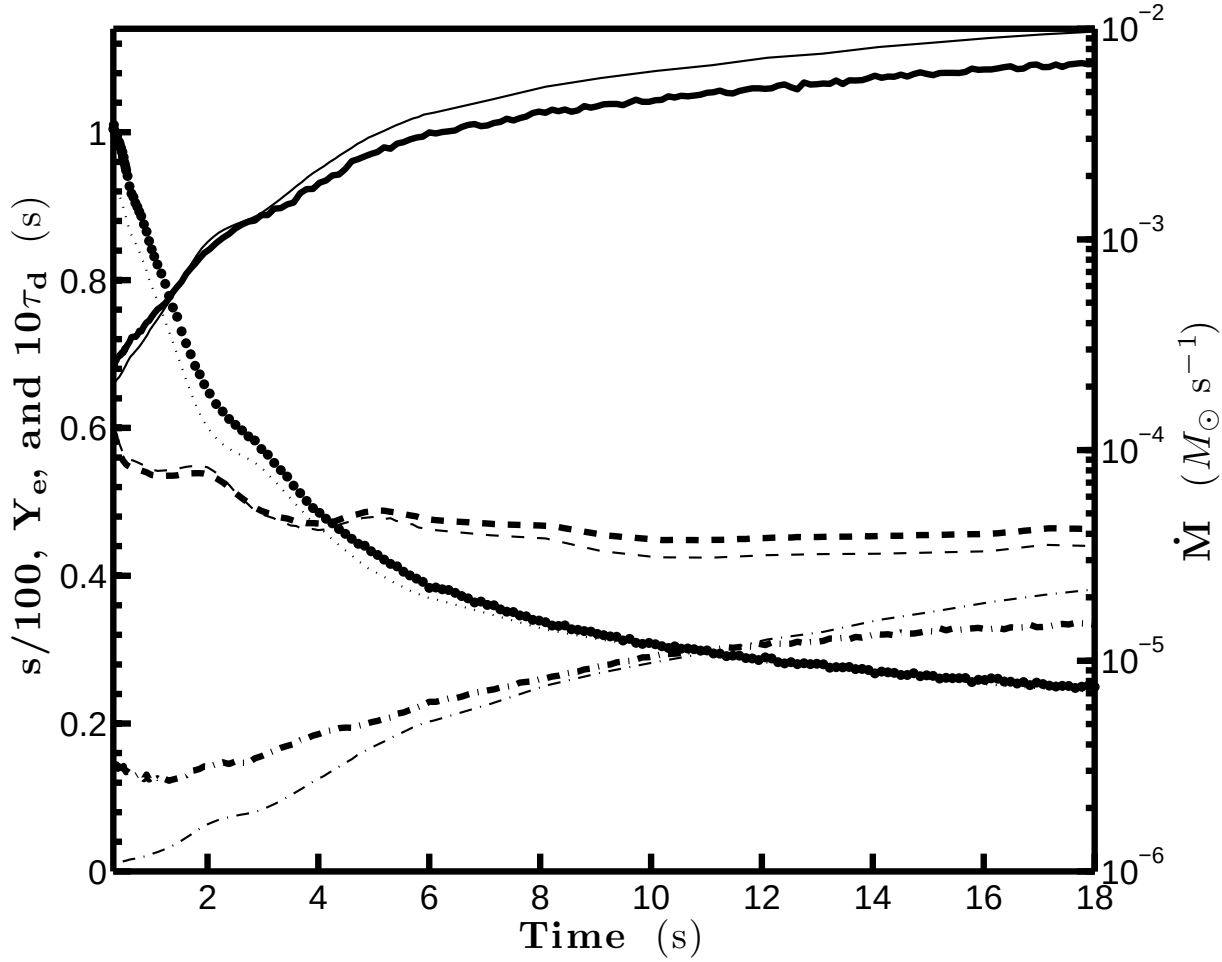

Fig. 4.— Properties of the neutrino driven wind from the Woosley et al. (1994) supernova model as a function of time. The thick lines correspond to the numerical results from Kepler and the thin lines correspond to the predictions of the analytic estimates described in the appendix. The solid line is the dimensionless entropy per baryon, the dashed line is the electron fraction, the dash dotted line is the dynamical timescale, and the dotted line is the mass loss rate. All of the quantities are taken extracted from where the wind temperature reaches 2 GK.

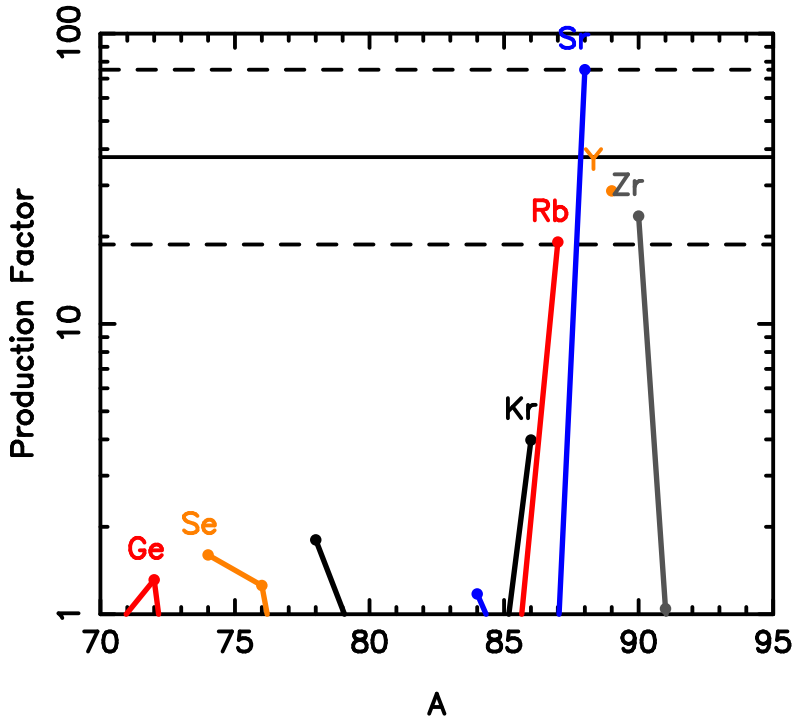

Fig. 5.— Isotopic production factors from the NDW model when the neutrino luminosities from Woosley et al. (1994) are used. The production factors are calculated assuming that 18.4 $M_{\odot}$ of material was ejected in the supernova in addition to the wind. The top dashed line corresponds to the greatest production factor in the wind, the solid line is a factor of two below that, and the bottom dashed line is a factor of two below the solid line. These lines specify an approximate coproduction band for the wind alone.

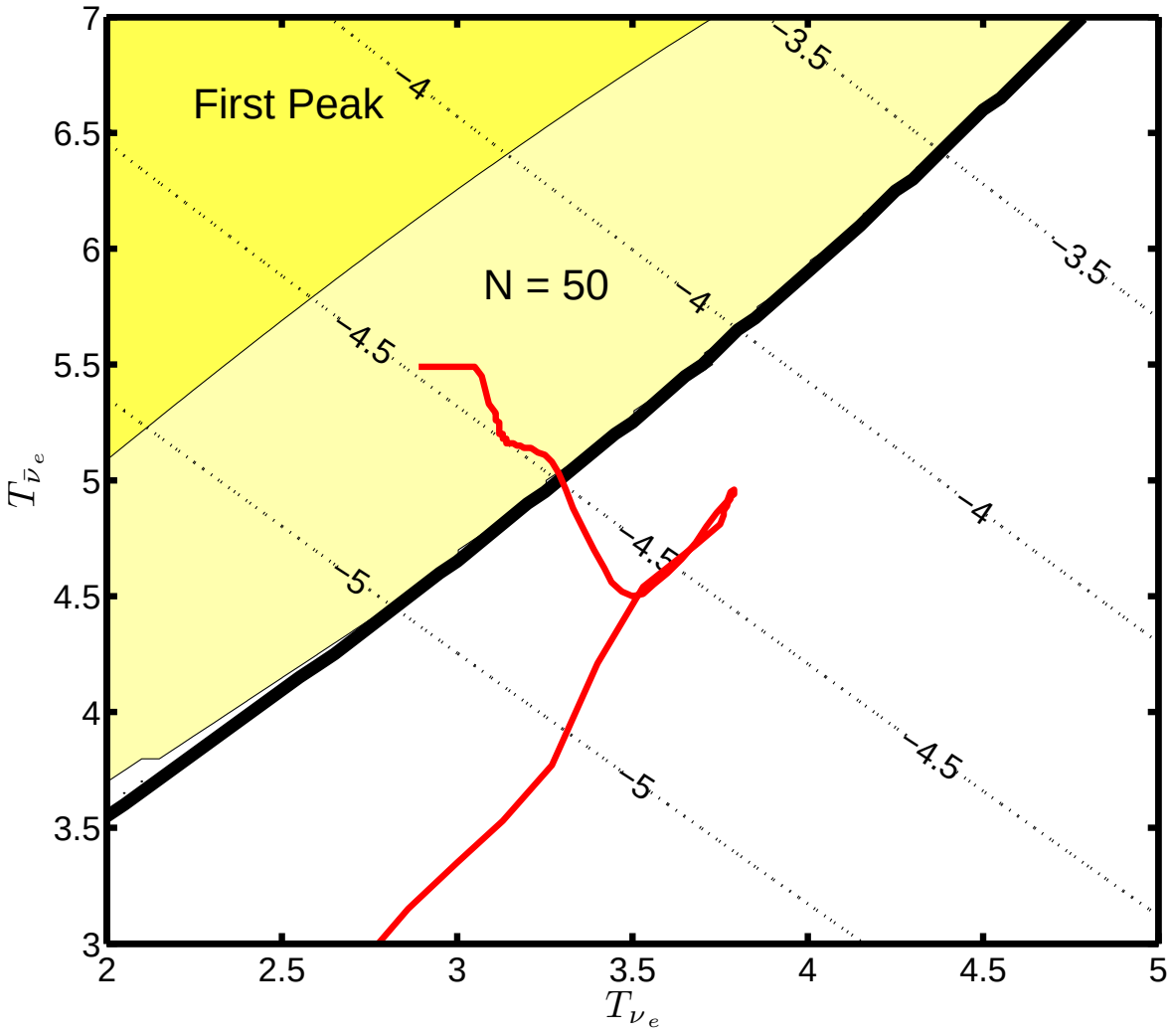

Fig. 6.— Neutrino two-color plot when the anti-neutrino luminosity is 1.2 times neutrino luminosity, and the total luminosity scales with average temperature to the fourth. Similar to figure 1. The red line is the neutrino temperatures from Woosley et al. (1994).

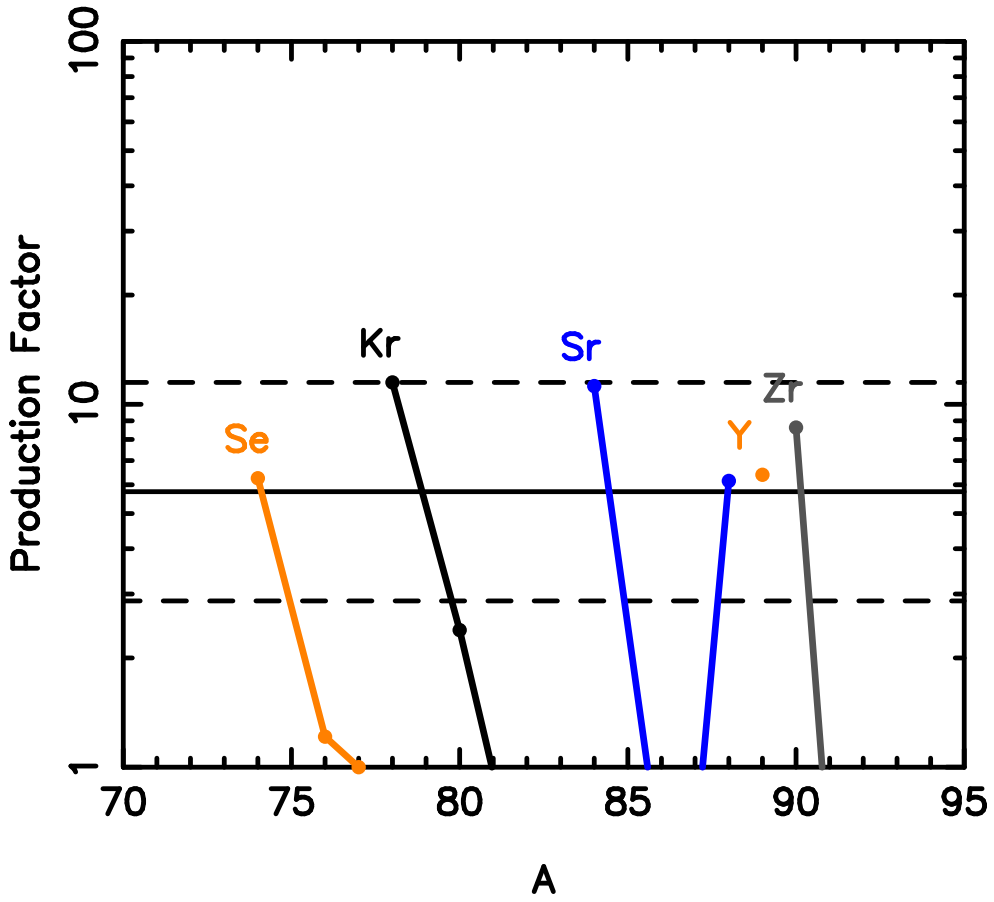

Fig. 7.— Isotopic production factors from the NDW model employing the neutrino luminosities from Woosley et al. (1994) with the anti-electron neutrino temperature reduced by 15%. The production factors are calculated assuming that $18.4\,M_{\odot}$ of material was ejected in the supernova in addition to the wind. The horizontal lines are similar to those in figure 5.

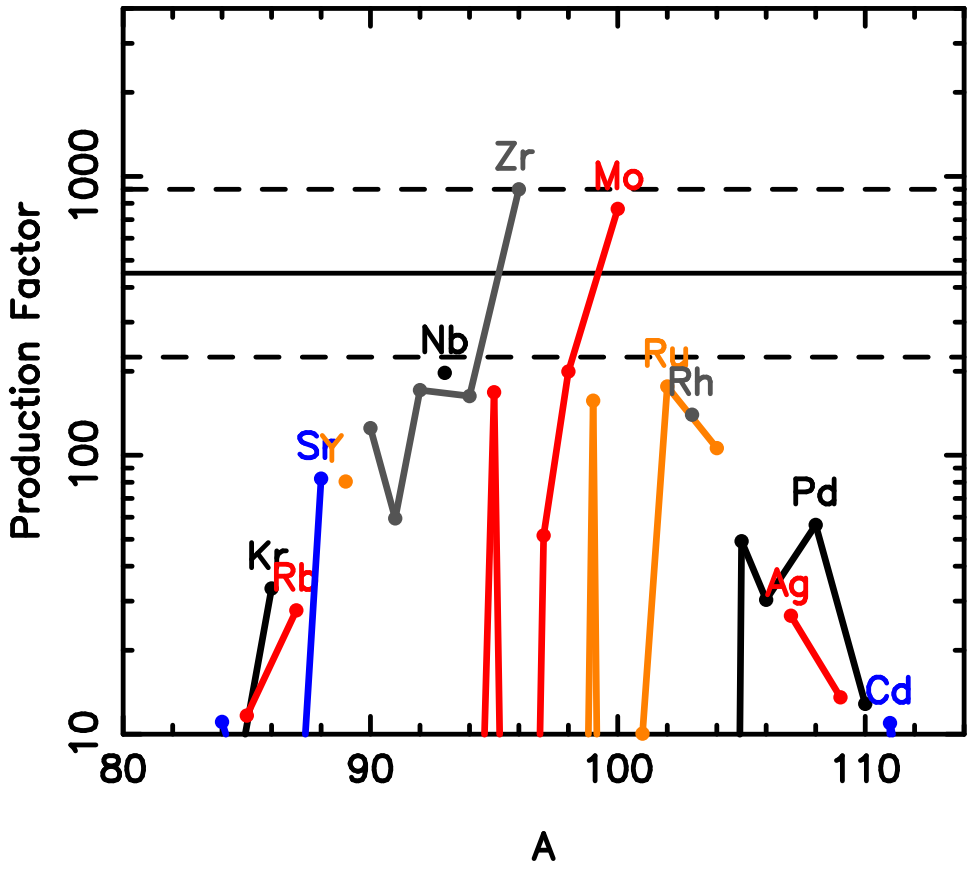

Fig. 8.— Isotopic production factors from the NDW model employing the neutrino luminosities from Woosley et al. (1994) with weak magnetism corrections turned off. The production factors are calculated assuming that $18.4\,M_\odot$ of material was ejected in the supernova in addition to the wind. The horizontal lines are similar to those in figure 5.

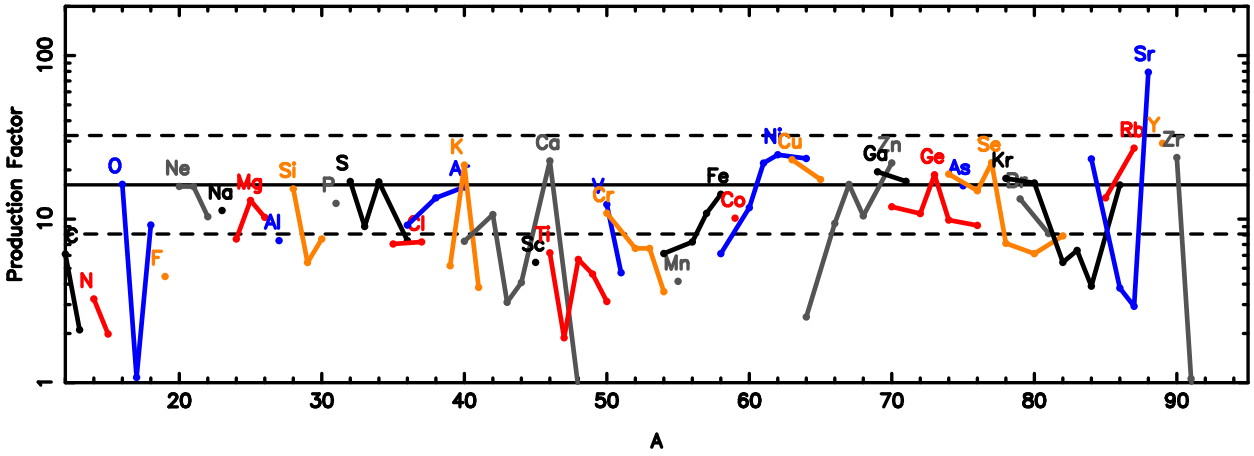

Fig. 9.— Combined isotopic production factors of the neutrino driven wind with unaltered neutrino temperatures and including weak magnetism corrections added to those of a $20M_{\odot}$ stellar model from Woosley & Weaver (1995). The solid black line is the coproduction line with ^{16}O. The dashed lines are a factor of two above and below the coproduction line. The neutrino driven wind is responsible for the production of ^{88}Sr, ^{89}Y, and ^{90}Zr.

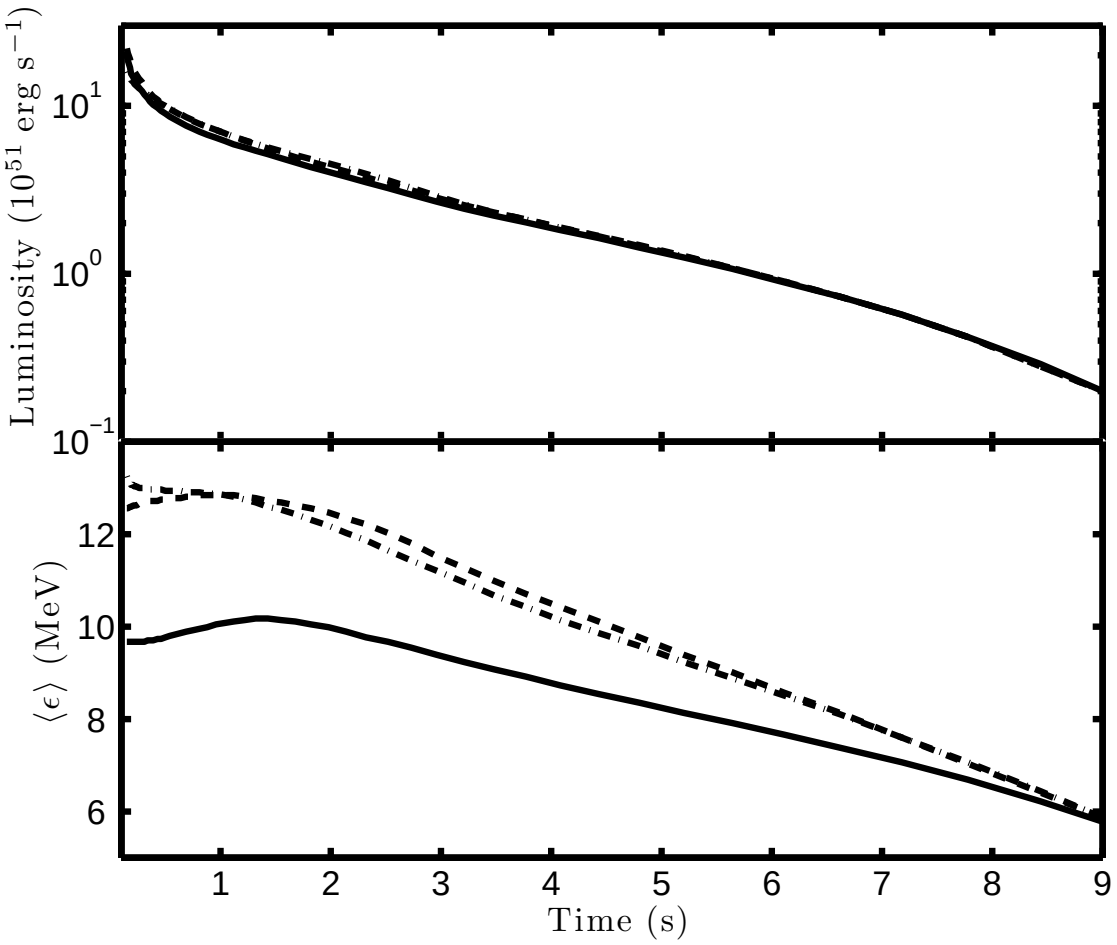

Fig. 10.— Neutrino luminosities and temperatures taken from the model of Huedepohl et al. (2009). The line styles are the same as in figure 2.

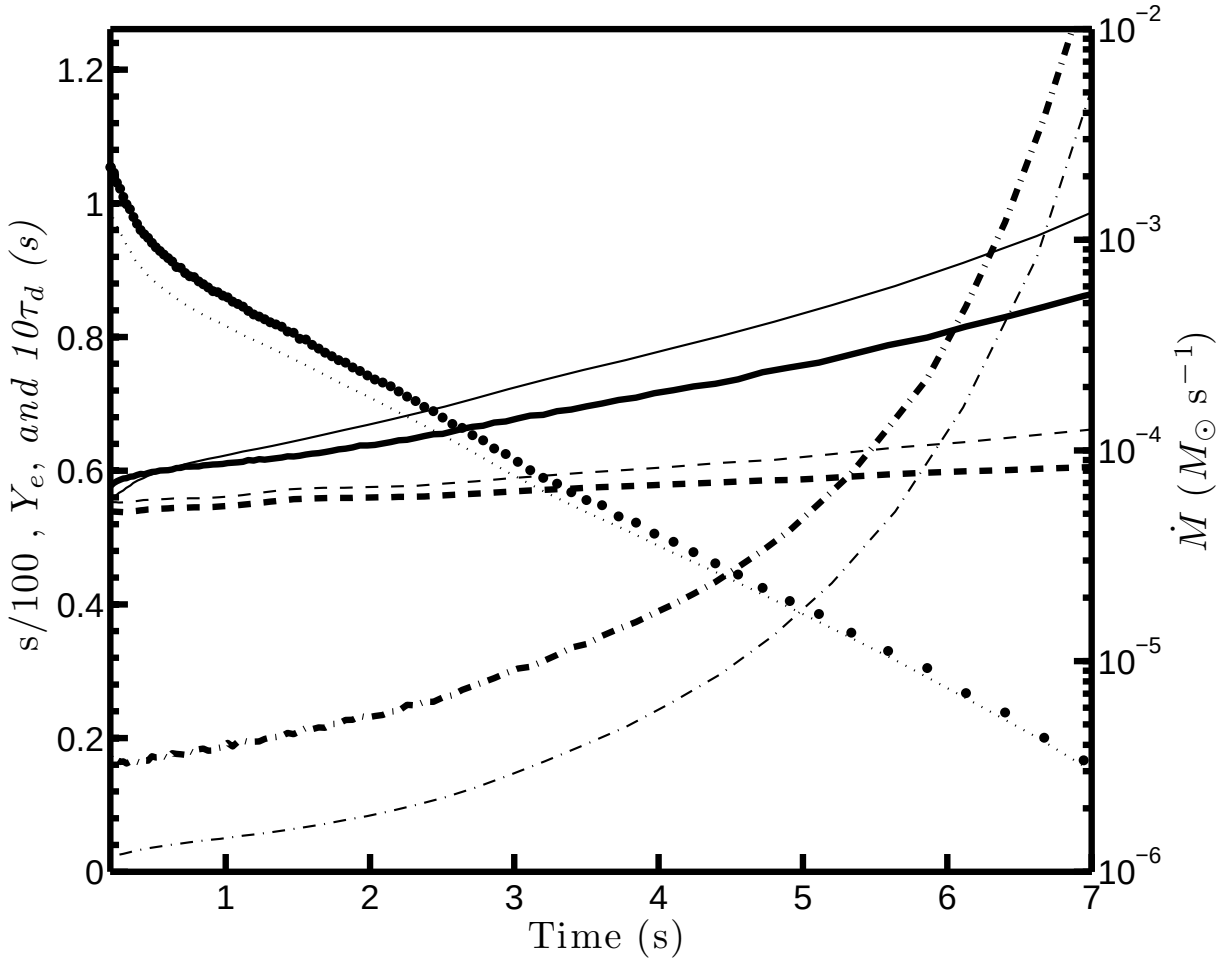

Fig. 11.— Properties of the neutrino driven wind from the Huedepohl et al. (2009) supernova model as a function of time. The lines have the same meaning as in figure 4.

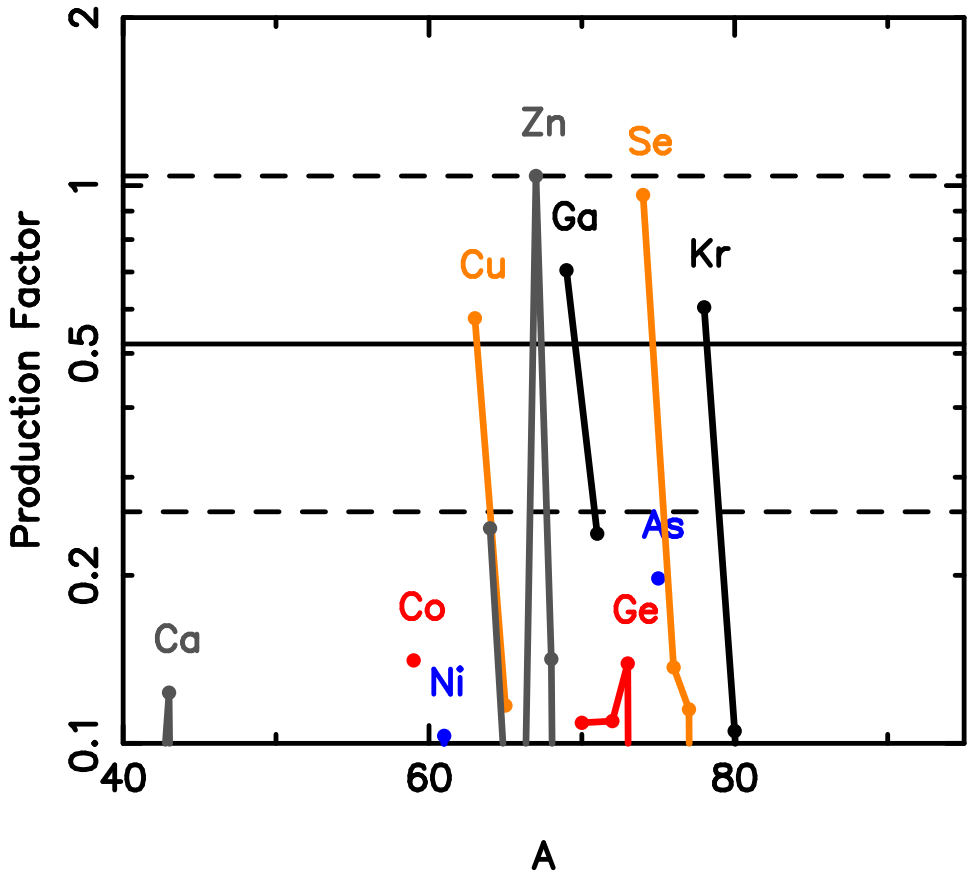

Fig. 12.— Isotopic production factors from the NDW model employing the neutrino luminosities from Huedepohl et al. (2009). The production factors are calculated assuming that $7.4\,M_{\odot}$ of material was ejected in the supernova in addition to the wind. The horizontal lines are similar to those in figure 5. Notice that none of the production factors are significantly greater than one.